

**Dynamics of methane ebullition from a peat monolith revealed  
from a dynamic flux chamber system**

**By**

**Zhongjie Yu**

**A Dissertation submitted to the**

**Graduate School-Newark**

**Rutgers, The State University of New Jersey**

**in partial fulfillment of the requirements**

**for the degree of**

**Master of Science**

**Graduate Program in**

**Environmental Sciences**

**written under the direction of**

**Professor Lee D. Slater**

**and approved by**

---

---

---

**Newark, New Jersey**

**January, 2014**

© [2014]

**Zhongjie Yu**

**ALL RIGHTS RESERVED**

## **ABSTRACT OF THE DISSERTATION**

### **Dynamics of methane ebullition from a peat monolith revealed from a dynamic flux chamber system**

By Zhongjie Yu

Dissertation Director:

Professor Lee D. Slater

Methane (CH<sub>4</sub>) ebullition in northern peatlands is poorly quantified in part due to its high spatiotemporal variability. In this study, we employed a continuous measurement approach to better understand the coupling between CH<sub>4</sub> ebullition fluxes and subsurface gas bubble dynamics and to examine potential triggering effects of atmospheric pressure and temperature on ebullitive CH<sub>4</sub> releases. A dynamic flux chamber system (DFC), consisting of a flow-through gas chamber and a fast methane analyzer (LI-COR 7700), was used to continuously measure CH<sub>4</sub> fluxes from a monolith of near-surface *Sphagnum* peat over eight weeks. By using a graphical separation method, episodic ebullition fluxes were extracted from total flux recorded, and the timing and CH<sub>4</sub> content of individual ebullition events identified. Coincident transmission ground penetrating radar (GPR) measurements of gas content and dissolved CH<sub>4</sub> concentrations in pore water were also acquired at three depths (upper, middle, and lower) within the monolith. Estimated episodic ebullition fluxes were not sensitive to the uncertainties in steady flux

quantification associated with the graphical model and the application of the DFC had minimal disturbance on air-peat CH<sub>4</sub> exchange. Episodic and steady ebullition fluxes, constrained by modeled diffusion fluxes using Fick's law and the bulk CH<sub>4</sub> concentrations in peat, were estimated as on average 38% and 36% of the total fluxes over the entire study period, respectively. The observations of gas content variations within the three layers along with the timing of episodic ebullition fluxes support the existence of an ebullition threshold regulating CH<sub>4</sub> ebullition. However, a larger threshold (gas content of 0.14 m<sup>3</sup> m<sup>-3</sup>) was found for the middle and lower layers, suggesting that multiple mechanisms related to the depth variation of peat structure were responsible for the complex behavior of episodic CH<sub>4</sub> ebullition. Temperature variation (23 °C to 27 °C) was likely only responsible for small episodic ebullition events from the upper peat layer, while large ebullition events from the deeper layers were most likely driven by drops in atmospheric pressure.

## **Acknowledgements**

I gratefully acknowledge the continuous support of my advisor, Professor Lee Slater. I really appreciate the opportunities you provided me and your encouragement, guidance and critical reviews of my work. I am also grateful to my thesis committee members, Professor Karina Schäfer and Professor Andrew Reeve (University of Maine), for providing valuable critiques at different stages of my research in last two years.

I also like to thank all the faculty and staff at the Department of Earth and Environmental Sciences, especially Ms. Liz Morrin for her support in all administrative aspects regarding class enrollment, ordering products and materials for my research. My appreciation goes to Professor Ruth Varner (University of New Hampshire) for her generous offer of instruments for my research.

I am thankful to all the members in Near Surface Geophysics Group and my fellow graduate students at the Department for their support, encouragement and the opportunities to learn from their experiences and skills. My thanks goes especially to Neil Terry for his valuable support during my field work in Caribou Bog, Maine. My thanks go also to the students Wagner Alcivar, Deborah Gonzalez, Barbara Goldman, and Adriana Morocho for their help with the field work. I am appreciative of Professor Dongqi Wang (ECNU, China) for providing valuable review comments on some of my manuscripts.

I would also like to acknowledge the financial support of Professor Lee Slater's National Science Foundation project (EAR-1045084) to this research work.

Finally, I am indebted to my girlfriend Ying Zhu for her support during this journey. I like to especially thank my parents for their support, love, understanding and sacrifices during my study in USA.

## Table of Contents

1. Introduction.....	1
2. Methods.....	6
2.1. Sample collection and preparation.....	6
2.2. DFC setup and flux calculation.....	7
2.3. CH <sub>4</sub> concentration corrections.....	10
2.4. Flux partitioning and ebullition extraction.....	12
2.5. CSC measurements.....	14
2.6. GPR measurements.....	15
2.7. Dissolved CH <sub>4</sub> concentration measurements.....	16
2.8. Modeling CH <sub>4</sub> diffusion fluxes from the peat.....	17
2.9. Experimental procedure.....	18
2.10. Data statistics.....	19
3. Results.....	21
3.1. Peat properties.....	21
3.2. Incubation conditions.....	21
3.3. Gas content and dissolved CH <sub>4</sub> concentrations.....	22
3.4. CH <sub>4</sub> fluxes measured using CSC.....	24
3.5. Modeled CH <sub>4</sub> diffusion fluxes.....	24
3.6. CH <sub>4</sub> fluxes measured using DFC.....	24
4. Discussion.....	30
4.1. Reliability of DFC in continuously monitoring CH <sub>4</sub> ebullition.....	31

4.2. Couplings between CH <sub>4</sub> ebullition and subsurface CH <sub>4</sub> dynamics.....	34
4.3. Relative importance of atmospheric pressure and temperature as ebullition triggers.....	40
5. Conclusions.....	43
References.....	44
Appendix.....	49
Curriculum vitae.....	58

## List of Illustrations

Figure 1: (A) dynamic flux chamber setup for continuous monitoring of CH <sub>4</sub> ebullition in the laboratory; (B) a picture showing side view of the stratum characteristics for the three layers.....	7
Figure 2: (A) flowchart of procedure for data correction, calculation, and extraction. (B) an example of the dynamics of CH <sub>4</sub> flux observed using DFC.....	11
Figure 3: Averaged 10-minutes temperature and relative humidity in gas chamber and averaged $C_{in}$ for every minute. ....	22
Figure 4: Gas content (A), dissolved CH <sub>4</sub> concentrations (B), steady and ebullition fluxes, ebullition frequency, and modeled diffusion fluxes (C) for each experimental day.....	23
Figure 5: Relationships among gas content, dissolved CH <sub>4</sub> concentrations, and ebullition fluxes and frequency for three layers.....	26
Figure 6: Frequency distribution of ebullitive CH <sub>4</sub> releases observed during the entire study period (n=926).....	27
Figure 7: Ebullitive CH <sub>4</sub> releases and atmospheric pressure as a function of time. The top 5% ebullitive CH <sub>4</sub> releases are shown in red.....	28
Figure 8: (A) and (B) ebullitive CH <sub>4</sub> releases observed in every experimental hour for week 2 to week 5 and week 6 to week 8, respectively. (C) and (D) relationships between cumulative ebullitive CH <sub>4</sub> release (filled diamond), cumulative number of ebullition (open cycle) and change in atmospheric pressure for week 2 to week 5 and week 6 to week 8, respectively.....	29

Fig. 9: Propagated error in calculated episodic ebullition fluxes by using the graphical model (error bars) and relationship between ebullition frequency and the ratio of ebullition flux to total flux (red dots).....	31
Fig. 10: Partitioned diffusion flux, steady ebullition flux, and episodic ebullition flux for each experimental day.....	33

## **List of Tables**

Table 1: Gas content, dissolved CH <sub>4</sub> , ebullition flux and its controls from peatland studies.....	2
Table 2: Data acquisition procedure for every experimental week.....	20

## 1. Introduction

Northern peatlands are a global methane ( $\text{CH}_4$ ) source, accounting for 12.2% of global  $\text{CH}_4$  emissions to the atmosphere, and a net sink for atmospheric carbon dioxide [Wuebbles and Hayhoe, 2002]. Carbon cycling in these ecosystems is controlled by the interactions among microbiological [Turetsky et al., 2008], hydrogeological [Slater and Reeve, 2002], plant ecological [Riutta et al., 2007], and climatological processes [Bragazza et al., 2012], which all have the potential to affect  $\text{CH}_4$  production, oxidation and transport dynamics [Lai et al., 2009]. During the last two decades there has been a growing interest in biogenically produced gas bubbles in northern peatlands. The presence of these bubbles in peat below the water table impacts the buoyancy of floating peat [Fechner-Levy and Hemond, 1996], results in the development of over-pressured stratum [Rosenberry et al., 2003], decreases hydraulic conductivity and substrate delivery [Kellner et al., 2005], and contributes to  $\text{CH}_4$  release from peatlands via rapid bubbling (ebullition) [Glaser et al., 2004]. Compared to other  $\text{CH}_4$  transport pathways in peatlands, i.e., diffusion of dissolved  $\text{CH}_4$  and venting of  $\text{CH}_4$  through aerenchyma of plants, ebullition of  $\text{CH}_4$ -containing bubbles from the subsurface might release larger amounts of  $\text{CH}_4$  and exhibit much greater spatiotemporal variations [Christensen et al., 2003]. This variability means that ebullition as a component of the total  $\text{CH}_4$  emissions from northern peatlands remains poorly quantified.

Theoretically, a bubble is formed in a fully saturated peat when the total pressure of the water-dissolved gases exceeds the sum of hydrostatic pressure imposed by the water table and atmospheric pressure [Strack et al., 2005]. Once formed in peat, biogenic bubbles can

be trapped under confining layers that consist of peat with pore diameters small enough to block the passage of bubbles [Rosenberry et al. 2003; Glaser et al., 2004]. Bubbles migrate upward to the water table once buoyancy forces surpass the trapping forces at the bubble-peat interface [Kellner et al., 2005]. Table 1 is a compilation of recent findings on CH<sub>4</sub> ebullition in peatlands obtained from various methods, showing that ebullition fluxes can vary over three or four orders of magnitude even under laboratory conditions, suggesting a variety of controlling factors (Table 1).

Table 1 Gas content, dissolved CH<sub>4</sub>, ebullition flux and its controls from peatland studies

gas content	dissolved CH <sub>4</sub> (mg L <sup>-1</sup> )	ebullition flux (mg m <sup>-2</sup> d <sup>-1</sup> )	controls on ebullition flux <sup>e</sup>	reference
0.01 - 0.15	0.1 - 11.7	2 - 83	bubble threshold	Baird et al. [2004]
		0 - 196	AT	Beckmann et al. [2004]
		45 - 225	surface vegetation	Christensen et al. [2004]
	0.1 - 1.3 <sup>b</sup>	3 - 68	AP	Comas and Wright [2012]
		0.2 - 784	surface vegetation	Green et al. [2012]
		<10	AP	Green et al. [2013]
0.02 - 0.16	11.7 - 13.9	49 - 152 <sup>a</sup>	CH <sub>4</sub> production, wind speed	Goodrich [2012]
		270	Bubble threshold, AP, AT	Kellner et al. [2006]
		7 - 12	none	Stamp et al. [2013]
0.05 - 0.15 <sup>c</sup>	0.1 - 5.8	65	AP, water table	Strack et al. [2005]
	~ 10.5 <sup>d</sup>	76 - 1233	AP	Tokida et al. [2005]
		48 - 1440	AP	Tokida et al. [2007]
0.03 - 0.15	1.0 - 11.6	1471 - 33093	AP, AT	Waddington et al. [2009]
0.04 - 0.15	0.1 - 11.2	0 - 237	AP, AT	this study

a: flux was obtained by multiplying seasonally-averaged ebullition event flux to mean CH<sub>4</sub> concentration for each event.

b: estimated from Figure 4 in the original paper.

c: change in volumetric gas content relative to the beginning point.

d: depth-averaged value, estimated by assuming partial pressure representing 45% by volume of CH<sub>4</sub> in bubbles.

e: AP and AT denote atmospheric pressure and atmospheric temperature, respectively.

One potential reason for the episodic nature of CH<sub>4</sub> ebullition is that a large bubble-storage capacity of peat may result in a partial decoupling between biological CH<sub>4</sub> production and bubble dynamics in subsurface peat [Strack and Waddington, 2008], such that physical factors can determine and/or alter the mechanical balance of the bubble-peat interaction, triggering ebullition [Tokida et al., 2009]. On the one hand, the physical properties of peat, such as degree of decomposition [Kettridge and Binley, 2011] and compressibility [Price et al., 2005], may set boundaries on the bubble trapping capacity and, subsequently, ebullition potential for peat. Results from laboratory incubations of near-surface *Sphagnum* peat suggest that there is a threshold gas content of 10 ~ 16% by volume, depending on the effective compressibility of peat, that must be reached in the peat matrix before the main period of ebullition [Baird et al., 2004; Kellner et al., 2006]. Changes in environmental factors, particularly atmospheric pressure and temperature (Table 1), may trigger ebullition through their direct impact on bubble volume as described by the Ideal Gas Law and Henry's Law [see Tokida et al. [2009] for a review]. Indeed, when the biological controls are steady state, CH<sub>4</sub> ebullition in northern peatlands can often be thought as a net consequence of mechanical disequilibrium associated with coupled below- and aboveground hydro-climatological changes.

Closed static chambers (CSC) and gas traps have been widely used to quantify ebullition fluxes in peatlands [e.g., Tokida et al., 2005; Stamp et al., 2013]. Stamp et al. [2013] reported a skewed spatial pattern of CH<sub>4</sub> ebullition in a raised bog based on 28 gas traps

with only 9 accounting for ~76% of the total seasonal flux. The large uncertainties associated with CH<sub>4</sub> ebullition estimates may in part result from a lack of suitable monitoring methods [Mastepanov and Christensen, 2009]. The CSC approach suffers from low temporal resolution, while gas traps only provide cumulative bubble volume trapped at the water table and thus indirect ebullition flux. In addition, neither of these two methods are able to clarify how individual ebullition events result from triggering factors over a long time scale. More recently, Goodrich et al. [2012], using automatic flux chambers with a high sampling frequency, observed a prominent diel variation of CH<sub>4</sub> ebullition in a temperate peatland over three seasons. This study highlighted the need for continuous flux measurements in order to obtain accurate ebullition estimates. Furthermore, although an ebullition threshold can be used to reasonably predict bubble release by volume in the laboratory [Kellner et al., 2006], it provides little insight into how physical characteristics of peat control the relationship between bubble accumulation and ebullition fluxes [Coulthard et al., 2009]. Continuous flux measurements are thus required to gain better process-based understanding of the complex behavior of CH<sub>4</sub> ebullition.

As a step towards better understanding of the importance of CH<sub>4</sub> ebullition fluxes, we developed a dynamic flux chamber (DFC) for the continuous monitoring of CH<sub>4</sub> ebullition from a near-surface peat monolith under laboratory conditions. A fast methane analyzer (FMA) providing high-precision and fast CH<sub>4</sub> concentration measurements was incorporated into the dynamic system for the quantification of both episodic CH<sub>4</sub> releases and integrated daily CH<sub>4</sub> ebullition estimates. Ground penetrating radar (GPR), a non-

invasive geophysical method for estimating gas content in peat [\[Comas and Slater, 2007\]](#) was also used, dissolved CH<sub>4</sub> concentrations in pore-water were measured. We first demonstrate the capacity of the set up and then use it to examine the dependence of CH<sub>4</sub> ebullition fluxes on subsurface bubble dynamics leading to insight into the underlying mechanisms triggering CH<sub>4</sub> ebullition in northern peatlands.

## 2. Methods

### 2.1. Sample collection and preparation

A peat monolith (c.  $394 \times 241 \times 330$  mm, surface area  $0.095 \text{ m}^2$ ) was extracted on November, 2012 from the surface of a lawn dominated by *Sphagnum* and low shrub in Caribou Bog, a large, multiunit freshwater bog complex in Maine. Vegetation on the surface of the monolith was left intact and consisted mainly of *Sphagnum* and ericaceous shrubs. The monolith was first removed from the field by inserting a mold of the same size ( $394 \times 241 \times 350$  mm) as the container used to hold the monolith (see below) into the ground and subsequently cutting and pulling back the surrounding peat, and cutting the base of the mold with a machete. The monolith was then placed into a temporary holder and transported back to the laboratory.

The monolith was pushed out from the mold into container made of 10 mm-thick transparent acrylic plastic. Three pore-water sampling ports were drilled vertically into one side of the container at 57 mm, 127 mm, 197 mm below the peat surface, representing an upper, middle, and lower layer of the peat monolith (Fig. 1). The exterior walls of the container were entirely covered by black tapes to prevent penetration of light and heat. This approach resulted in a tight interface between the peat monolith and the edge of the container, reducing the possibility of preferential transfer of gas bubbles up the container walls. Three pore-water samplers constructed from unglazed pipe (1.58 mm inner diameter) and fitted with a three-way stopcock were horizontally inserted into the ports. Distilled water was sprayed onto the peat surface to maintain saturated anaerobic

conditions in the peat. The peat monolith was maintained at room temperature (c. 22 ~ 24 °C).

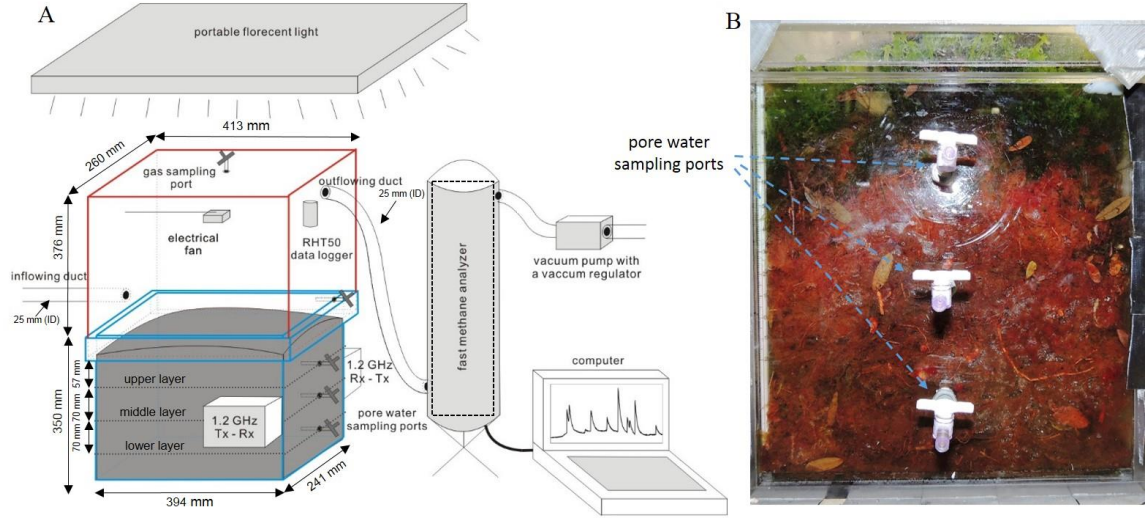


Figure 1 (A) dynamic flux chamber setup for continuous monitoring of CH<sub>4</sub> ebullition in the laboratory; (B) side view showing stratum characteristics for the three layers.

## 2.2. DFC setup and flux calculation

The DFC is a technique that has been developed to continuously measure earth-atmosphere fluxes of various compounds including CO<sub>2</sub> and CH<sub>4</sub> [Lai et al., 2012]. In contrast to the CSC technique, the DFC is designed to maintain a constant flow of outside air through the chamber enclosing the areas of interest. When the system operates under a dynamic equilibrium, the CH<sub>4</sub> flux ( $F$ , mg m<sup>-2</sup> min<sup>-1</sup>) from the monolith is associated with the concentration difference between the air entering ( $C_{in}$ , mg m<sup>-3</sup>) and leaving ( $C_{out}$ , mg m<sup>-3</sup>) the chamber headspace [Pape et al., 2009],

$$F = \frac{Q}{A} \times (C_{out} - C_{in}), \quad \text{Eq. 1}$$

where  $Q$  and  $A$  are the flow rate of purging air ( $\text{m}^3 \text{ min}^{-1}$ ) and surface area ( $\text{m}^2$ ) of the peat monolith, respectively.

A DFC requires careful system design to achieve minimal modification of the soil-air  $\text{CH}_4$  exchange regime. In this study, we modified the DFC system described in Mastepanov and Christensen [2009] by employing a LI-7700 open path fast methane analyzer (FMA, LI-COR Biosciences, Lincoln, NE, USA) to determine  $\text{CH}_4$  concentration. This DFC system consisted of a gas chamber ( $413 \times 260 \times 325 \text{ mm}$ ) that can be fitted to the water-filled collar on the top of the peat container for gas flux measurement (Fig. 1A). The chamber was made of 10 mm-thick transparent acrylic plastic with a headspace volume of  $0.035 \text{ m}^3$ . Inflow and outflow air ducts (25 mm inner diameter and 0.5 m length), a gas sampling port and a standpipe for regulating the water table of peat monolith was installed (Fig. 1A). The inflow duct was located 0.09 m above the peat surface, with the outflow duct 0.32 m above the peat surface on the opposite side of chamber (Fig. 1A). A steady purging flow of  $0.0047 \text{ m}^3 \text{ min}^{-1}$  was maintained by a vacuum pump with a vacuum regulator (Fig. 1A). This flow rate resulted in a mean residence time of air in the chamber of 7.5 minutes, being in the middle of the range of residence times reported in the literature [Table 4 in Pape et al., 2009] and considered a good compromise between flux detection limit and time response of the system. Preliminary tests confirmed that this setup caused no significant pressure difference between the chamber and the laboratory (data not shown for brevity). Turbulent mixing inside the gas chamber was encouraged using an electric fan blowing downwards (Fig. 1A). The approach promoted mixing of the air in the chamber headspace such that the

CH<sub>4</sub> could be assumed uniform throughout the chamber headspace. The continuous measurement of  $C_{out}$  then provides information on CH<sub>4</sub> dynamics in the chamber [Pape et al., 2009].

The LI-7700 open path FMA is a high-speed, high-precision, wavelength modulation spectroscopy-based CH<sub>4</sub> analyzer [McDermitt et al., 2011]. Its root mean square noise is 5 ppb for a 10 Hz measurement at typical ambient CH<sub>4</sub> concentrations (~2 ppm). In this study, we modified the data acquisition mode of the LI-7700 FMA by enclosing it within the calibration shroud provided by the manufacturer, resulting in a closed inner cell ( $V_{FMA}$ , 0.009 m<sup>3</sup>) as the terminal space for CH<sub>4</sub> analysis. The FMA was positioned in series with the gas chamber and the vacuum pump (Fig. 1a). After leaving the gas chamber, the purging air flows into the inner cell via the bottom fitting and then leaves through the top fitting at the same flow rate as applied to the gas chamber. Since the volume of the inner cell is much smaller than the gas chamber, complete mixing is insured in the inner cell space. By assuming steady state condition in the inner cell, a CH<sub>4</sub> mass balance can relate  $C_{out}$  to CH<sub>4</sub> concentrations recorded by the FMA in the inner cell,

$$(C_{out} - C_i) \times V_{out} = (C_{i+1} - C_i) \times V_{FMA} \quad \text{Eq. 2}$$

where  $C_i$  and  $C_{i+1}$  are CH<sub>4</sub> concentrations in the inner cell (mg m<sup>-3</sup>) recorded at time moment  $i$  and  $i+1$ , respectively, and  $V_{out}$  is the volume of outflowing air entering the inner cell over the time period from  $i$  to  $i+1$  (m<sup>3</sup>). Consequently,  $C_{out}$  can be inversely calculated from the FMA time series of inner cell concentration collected at 5 Hz.

Uncertainties in calculated  $C_{out}$  and  $\text{CH}_4$  fluxes were estimated using Gaussian error propagation [Oswald et al., 2013],

$$\Delta C_{out} = \sqrt{\left[ \left( \frac{\partial C_{out}}{\partial V_{FMA}} \right)_{V_{out}, C_{i+1}, C_i} \cdot \Delta V_{FMA} \right]^2 + \left[ \left( \frac{\partial C_{out}}{\partial V_{out}} \right)_{V_{FMA}, C_{i+1}, C_i} \cdot \Delta V_{out} \right]^2 + 2 \cdot \left[ \left( \frac{\partial C_{out}}{\partial C_{i+1}} \right)_{V_{out}, V_{FMA}, C_i} \cdot \Delta C_{i+1} \right]^2} \quad \text{Eq. 3}$$

$$\Delta F = \sqrt{\left[ \left( \frac{\partial F}{\partial Q} \right)_{A, C_{out}, C_{in}} \cdot \Delta Q \right]^2 + \left[ \left( \frac{\partial F}{\partial A} \right)_{Q, C_{out}, C_{in}} \cdot \Delta A \right]^2 + 2 \cdot \left[ \left( \frac{\partial F}{\partial C_{out}} \right)_{Q, A, C_i} \cdot \Delta C_{out} \right]^2} \quad \text{Eq. 4}$$

The error in bulk  $\text{CH}_4$  concentrations ( $\Delta C_{i+1}$ ) was set to the noise of the instrument under ambient  $\text{CH}_4$  concentrations [Oswald et al., 2013] measured in the laboratory. The errors for the purging air flow rate ( $\Delta Q$ ) and outflowing air volume ( $\Delta V_{out}$ ) were estimated from the standard deviation of the measured flow rate using a gas flow meter. The errors for the soil surface area ( $\Delta A$ ) and volume of the inner cell ( $\Delta V_{FMA}$ ) were determined from a length measurement.

### 2.3. $\text{CH}_4$ concentration corrections

The determination of  $C_{out}$  by the FMA is affected by variations of temperature and water vapor via thermal expansion and water vapor dilution; in addition, temperature, pressure, and water vapor density in the inner cell impact concentration measurement by shifting the spectroscopic light absorption of the FMA [McDermitt et al., 2011]. In order to take these effects into account, one RHT50 data logger (Extech Instruments, USA) was installed right beside the outflowing duct in the gas chamber to measure temperature, atmospheric pressure, and relative humidity of the chamber headspace every 10 minutes. Another identical RHT50 data logger was installed in the laboratory to measure ambient

conditions for comparison. As the FMA was connected to the gas chamber for more than five days per experiment (see below), it is reasonable to assume that the inner cell quickly reached a dynamic equilibrium with the gas chamber in terms of water vapor density. The raw bulk  $\text{CH}_4$  concentration data were corrected by using 10-minute averaged water vapor densities converted from the relative humidity of the chamber headspace, and FMA measured temperature and pressure according to the Webb-Pearman-Leuning (WPL) corrections [Webb et al., 1980] and spectroscopic correction [McDermitt et al., 2011] prior to  $C_{out}$  inversion. Figure 2A summarizes the sequence of the data correction and calculation steps described above, and Fig. 2B shows a typical flux dataset obtained from the DFC system.

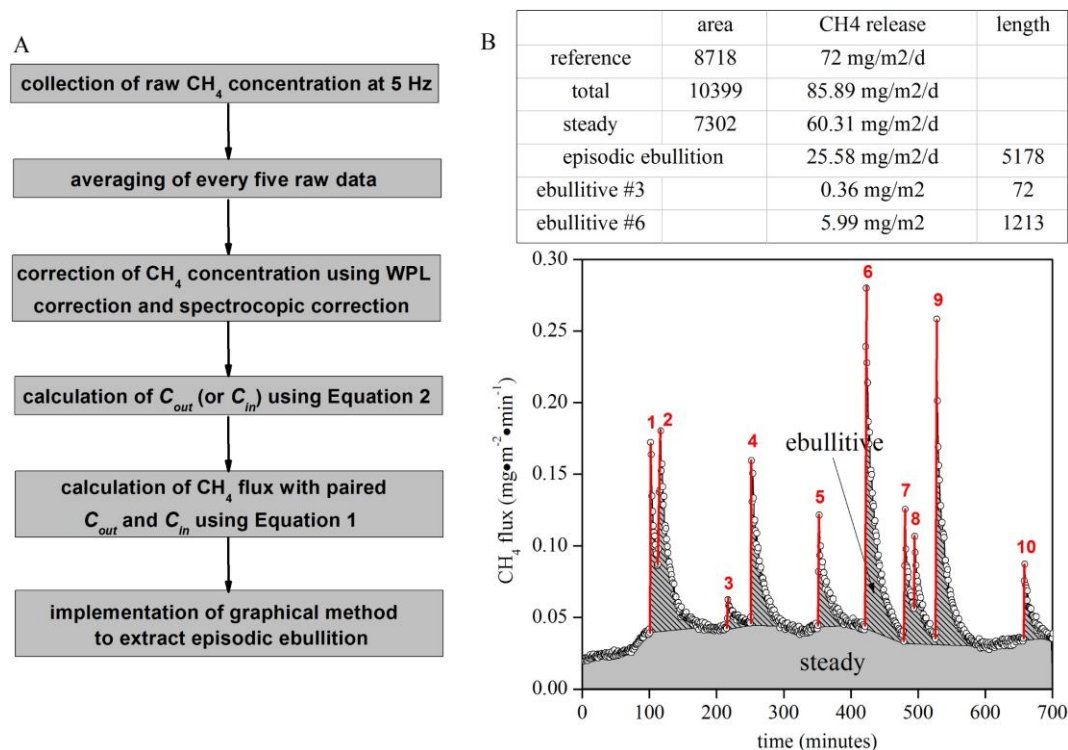


Figure 2 (A) flowchart of procedure for data correction, calculation, and extraction. (B) an example of the dynamics of  $\text{CH}_4$  flux observed using DFC. Steady flux (gray areas)

and episodic ebullition flux (shaded area) were separated and identified using a graphical model. Ten ebullitive  $\text{CH}_4$  releases were identified (straight red lines). Calculations of ebullition flux and ebullitive  $\text{CH}_4$  release are shown in the table.

## **2.4. Flux partitioning and ebullition extraction**

Based on distinctions in temporal continuity, diffusion and plant-mediated transport are usually classified as steady emission pathways, while ebullition is conventionally considered as random in time. However, recent studies suggest that in peatlands  $\text{CH}_4$  ebullition can also occur in a steady manner over time frames of minutes to hours [Coulthard et al., 2009]. In some studies, diffusion, plant-mediated transport, and steady ebullition are collectively defined as steady emission, while ebullition occurring in short-lived bursts or episodes where fluxes are generally much higher and more variable than background steady fluxes are termed episodic ebullition [Green and Baird, 2012]. In this study, we follow such definitions to partition measured  $\text{CH}_4$  fluxes.

Using the DFC system, the frequency of episodic ebullition during a specific time period can be determined by visual counting of flux peaks in flux time series (Fig. 2B). Ideally, episodic ebullition fluxes can also be accurately separated out from steady fluxes as outliers in the flux dynamics. However, such situation requires a gas residence time of DFC as short as that necessary for a released gas bubble to disseminate its content throughout the chamber headspace, which is not feasible in practice with the consideration of achieving a minimal perturbation of pressure regime in the headspace. Since some accumulation of ebullition-derived  $\text{CH}_4$  in the gas chamber is unavoidable,

the calculated fluxes from the DFC system are apparent fluxes rather than instantaneous  $\text{CH}_4$  emission rates from the peat monolith. In this sense, episodic ebullition fluxes are best isolated from the baseline steady fluxes by integrating areas under ebullition flux peaks [Panikov et al., 2007] (Fig. 2B).

Methods exist to statistically identify a baseline in a time series and quantitatively integrate area under peaks, e.g. chromatographic algorithms. However, these methods may only be applicable in cases where the baseline is stable [Panikov et al., 2007]. By using a similar flow-through system, Christensen et al. [2003] defined steady baselines visually with a fixed flux rate for individual datasets. In this study, we adopted a simple graphical model that is analogous to the hydrological approach for extracting peak flows in stream hydrographs. We defined the baselines by tracking the smooth variation in flux until first arrival of a peak and identifying the point at which the peak returned to a steady state, such that the baseline was set as a straight line under the peak (Fig. 2B). Calculated  $\text{CH}_4$  fluxes were first plotted in OriginPro 8.1 (OriginLab Corporation, USA) and normalized to a standard axis format. The flux graphs were then imported into ImageJ for calculation of areas under peaks. Polygons were drawn to define areas under the baseline along with a reference rectangle of known flux in the standardized graphs, respectively, and their areas were automatically calculated (see inserted table in Fig. 2B). Steady flux can then be quantified by comparing its integrated area to the reference. The difference between total flux and steady flux gives the integrative episodic ebullition flux over the time period of interest. The accuracy of the estimated episodic ebullition flux was assessed by analyzing the potential error in the steady flux quantification.

Similar to other flow-through systems (e.g., inline membrane probes for *in situ* measurement of pore water chemistry [Mastepanov and Christensen, 2009]), the difference between peak height and baseline level is a good approximation of CH<sub>4</sub> content in individual episodic events. Once integrated episodic ebullition fluxes were extracted from the time series, we graphically measured the peak height from the starting point of a peak, which may be on the baseline or on the declining slope of the immediately prior peak when two peaks occur closely in time (e.g., later phase in Fig. 2B), to its highest point in the standardized graphs (Fig. 2B). Individual peak heights were then compared to total lengths over a certain time period to calculate ebullitive CH<sub>4</sub> release for each episodic ebullition events. All original flux data, showing the defined baseline and identified peak heights are provided in the appendix.

## 2.5. CSC measurements

The gas chamber of the DFC system was modified for CSC measurements of steady fluxes by closing the inflow and outflow holes with fittings and extending the water resupply tube to be a vent tube for pressure balance. For each CSC measurement, a 30 minutes chamber closure time was adopted; seven 30 mL gas samples were taken from the top sampling port at a 5 minute time interval after chamber closure and injected into pre-vacuumed 20 mL vials for gas chromatograph (Shimadzu, GC-14A, Japan) analysis. Linear regressions were performed on each set of CH<sub>4</sub> concentration series to calculate flux. The CSC flux measurement was accepted if the determination coefficient of linear regression ( $R^2$ ) is larger than 0.90.

## 2.6. GPR measurements

The theory and methods employed to use GPR to characterize gas bubble dynamics in peat soils have been documented elsewhere [e.g., Comas et al., 2007; Comas et al., 2008]. In this work, we modified a laboratory GPR system and data acquisition protocol initially used by Comas and Slater [2007], improving the accuracy of gas content estimates by replacing reflection-based measurements with transmission measurements.

A Mala-RAMAC GPR system equipped with a pair of 1.2-GHz shielded antenna was used to compute the velocity of EM waves in the upper, middle, and lower layers of the peat monolith (three lines as shown in Fig. 1a). Three horizontal positions spaced 0.1 m apart were used for a GPR measurement in each layer. EM waves were transmitted across the monolith and direct wave travel times, complete with reciprocal data for each location, recorded. The velocity ( $v$ ) of the EM wave in peat is calculated using the known distance that the EM wave traveled (i.e., across the length of the peat container).

Assuming a low-loss medium [Comas and Slater, 2007; Parsekian et al., 2012],  $v$  can then be simply converted to the bulk relative permittivity of the peat ( $\epsilon_{r(b)}$ ),

$$\epsilon_{r(b)} = \left(\frac{c}{v}\right)^2, \quad \text{Eq. 5}$$

where  $c$  is the EM wave velocity in a vacuum ( $3 \times 10^8 \text{ m s}^{-1}$ ).

The strong contrast in relative permittivity between air ( $\epsilon_{r(a)} = 1$ ) and water ( $\epsilon_{r(w)} = 79$  at laboratory temperature of 23 °C) forms the basis for using measurements of  $\epsilon_{r(b)}$  to determine gas content in peat soils. A multiphase dielectric mixing model variant of the

Complex Refractive Index Model (CRIM) was applied to estimate gas content [Parsekian et al., 2012],

$$\varepsilon_{r(b)}^\alpha = \theta \varepsilon_{r(w)}^\alpha + (1 - \phi) \varepsilon_{r(s)}^\alpha + (\phi - \theta) \varepsilon_{r(g)}^\alpha, \quad \text{Eq. 5}$$

where  $\varepsilon_{r(s)}$  is relative permittivity of the solid phase assumed here as 2 [Comas and Slater, 2007],  $\theta$  is the water content,  $\phi$  is porosity, and  $\alpha$  is an empirical coefficient related to the orientation of the electromagnetic waves to the peat particles. The term  $\phi - \theta$  is the volumetric gas content of the peat. In this study, we set the value of  $\alpha = 0.33$  as previously determined empirically for Caribou bog peat samples [Parsekian et al., 2012]. We assume that porosity did not change throughout the experiment due to container wall preventing horizontal peat deformation [Comas and Slater, 2007]. Thus, the porosity measured at the end of the incubation (see below) was used in Eq. 5 to calculate gas content for the entire study.

## 2.7. Dissolved CH<sub>4</sub> concentration measurements

To measure the dissolved CH<sub>4</sub> concentrations in pore-water, 2 mL of pore-water was collected by syringe from the samplers in the upper, middle, and lower layers respectively and injected into an 8 mL vial filled with ambient air. The vials were then shaken vigorously for 15 minutes to equilibrate CH<sub>4</sub> between the headspace and water phase. The CH<sub>4</sub> concentration in the headspace of the vial and two replicates of ambient air were determined by GC, and the original dissolved concentration was reconstructed using the headspace concentrations, the ambient CH<sub>4</sub> concentration, the volumes of the headspace and water phase, and temperature-corrected Bunsen solubility coefficient [Wiesenburg and Guinasso, 1979].

## 2.8. Modeling CH<sub>4</sub> diffusion fluxes from the peat

CH<sub>4</sub> diffusion fluxes across the soil surface can be theoretically calculated from the CH<sub>4</sub> concentration gradient within the soil using Fick's first law of diffusion [Reid et al., 2013]. In flooded peat, CH<sub>4</sub> diffusion occurs in both air-filled and water-filled pore space such that the presence of gas bubbles causes CH<sub>4</sub> diffusion fluxes much higher than modeled results that only consider dissolved CH<sub>4</sub> transport in pore water [Stephen et al., 1998a]. In this study, CH<sub>4</sub> diffusion fluxes from the peat monolith were modeled using Fick's first law with model coefficients specifically derived for flooded soil containing gas bubbles (Eq. 6),

$$F = D_e \frac{\partial C_b}{\partial z} \approx D_e \frac{C_b}{\partial z}, \quad \text{Eq. 6}$$

$$D_e \approx \left[ \frac{(\epsilon + \theta) \sqrt{D_a D_w}}{\epsilon \sqrt{D_w} + \theta \sqrt{D_a}} \right]^2, \quad \text{Eq. 7}$$

$$C_b = \epsilon C_a + \theta C_w = \left( \frac{\epsilon}{\alpha_b} + \theta \right) C_w, \quad \text{Eq. 8}$$

where  $D_e$  is the effective bulk diffusion coefficient and can be expressed as a function of the CH<sub>4</sub> diffusion coefficients in free air ( $D_a$ ) and water ( $D_w$ ), gas content ( $\epsilon$ ), and water content ( $\theta$ ) of the peat medium (Eq. 7) [Nielson et al., 1984; Stephen et al., 1998a]. The term  $\partial C_b / \partial z$  is the gradient of bulk CH<sub>4</sub> concentration over depth  $z$  to the water table. By assuming that equilibrium in the gas-pore water system can be reached rapidly and obeys Henry's law,  $C_b$  can be calculated using measured  $\epsilon$ ,  $\theta$ , dissolved CH<sub>4</sub> concentration ( $C_w$ ), and Bunsen solubility coefficient for CH<sub>4</sub> ( $\alpha_b$ ) according to Eq. 8 [Stephen et al., 1998a]. In the calculations using Eq. 6 a simplification was made because  $C_b$  in peat is much higher than the equilibrated CH<sub>4</sub> concentration at water table [Reid et al., 2013]. All diffusion and solubility coefficients used in this study were corrected for temperature.

An important boundary condition on Fick's first law is that the concentration gradient in soil has to be taken in the direction where it is steepest [Rothfuss and Conard, 1998]. Gas bubbles affect CH<sub>4</sub> concentration gradients in flooded soils and thus CH<sub>4</sub> diffusion modeling by (1) resulting in a three-dimensional uneven structure of CH<sub>4</sub> gradients in which the concentration isopaths follow the surface of trapped gas bubbles [Rothfuss and Conard, 1998] and (2) increasing dissolved CH<sub>4</sub> concentrations in shallower peat via re-dissolution during their migration toward the surface [Tang et al., 2010]. As a result, the distribution of CH<sub>4</sub> in flooded soil profile is highly variable even in layers right below the water table [Panikov et al., 2007], and any choice of depth in the calculation of concentration gradient will be arbitrary. For simplicity, we used average values of the three layers and set the lower boundary of the concentration gradient at the middle layer to model CH<sub>4</sub> diffusion flux for each experimental day.

## 2.9. Experimental procedure

As our goal was to understand how CH<sub>4</sub> ebullition depends on the evolution of biogenic bubbles in peat and how atmospheric pressure and temperature influence ebullition, we conducted the experiment, such that the whole experiment system was subject to natural fluctuations of atmospheric pressure and temperature of the laboratory. A fluorescent light was set up above the gas chamber for simulating a 12 hour day/night cycle with a daytime light intensity of 4350 Lux at the peat surface and providing additional heating that enhanced the amplitude of temperature variation in the gas chamber (Fig. 1A). Two days before the incubation, the peat monolith was drained by unscrewing three pore-

water samplers and gently tilting the peat container to pour the water out. We then slowly rewetted the peat monolith from the bottom pore-water sampling port using distilled water until the water table was 2 cm below the peat surface. The rewetting encouraged a low initial  $\text{CH}_4$  level and gas content in peat. One set of GPR measurements, one round of pore water sampling, and three sets of CSC flux measurements were taken immediately after the rewetting to establish pre-incubated conditions. During the entire study period, the water table was maintained at its initial level by replenishing with distilled water through the water filling tube.

Eight consecutive weeks of  $\text{CH}_4$  ebullition monitoring began on March 26, 2013. For every experimental week, the DFC system was started 12 hours before the continuous flux monitoring in order to establish dynamic equilibrium. Details of the data acquisition procedure for every experimental week are summarized in Table 2. Importantly,  $C_{out}$  was continuously measured for 120 hours every experimental week under continuous chamber closure, and measured  $C_{in}$  values were averaged to one 24-hour dataset and then used to calculate flux for every experimental day. After eight weeks of flux monitoring, three replicate samples were extracted from the upper, middle, and lower layers of the monolith respectively by cutting from the surface. Then, the humification degree, stratum characteristics, bulk density, and porosity were measured using a weight loss on drying procedure previously used by Comas and Slater [\[2007\]](#).

Table 2 Data acquisition procedure for every experimental week

Day 1 – Day 5	Day 6	Day 7
<ul style="list-style-type: none"> <li>• <math>C_{out}</math> from the gas chamber was continuously measured under 5 day/night cycles (120 h)</li> <li>• GPR and pore-water samplings at three layers were conducted twice a day during daytime</li> </ul>	FMA was disconnected from the gas chamber to measure $C_{in}$ for 24 h	three sets of CSC flux measurement were taken during daytime

### 2.10. Data statistics

The corrections and calculations of all CH<sub>4</sub> fluxes were performed in MATLAB (Mathworks, USA), and all data statistical tests were performed using SPSS (SPSS Inc., USA). A one-way ANOVA followed by Fisher's least significant difference test for pairwise comparison was used to determine significant differences between independent variables. Simple linear regression and Pearson's Correlation Coefficient were used to detect significant relationships among independent variables.

### 3. Results

#### 3.1. Peat properties

The von Post humification test indicated that the upper layer of the monolith was undecomposed (H2), while the middle and lower layers were slightly decomposed (H3-H4). Below the upper layer, *Sphagnum* accumulated with slightly decomposed branches, stems, and variable amounts of woody material (Fig. 1B). Bulk density was found to be  $0.052 \text{ g cm}^{-3}$ ,  $0.065 \text{ g cm}^{-3}$ , and  $0.078 \text{ g cm}^{-3}$  for the upper, middle, and lower layers, respectively. Porosity for the upper, middle, and lower layers were 0.96, 0.95, and 0.94, respectively.

#### 3.2. Incubation conditions

The temperature in the gas chamber exhibited significant diel patterns (Fig. 3). Averaged 10-minute temperatures were  $23^{\circ}\text{C}$  to  $24^{\circ}\text{C}$  during nighttime, increasing to  $26^{\circ}\text{C}$  to  $27^{\circ}\text{C}$  when the florescent light was on. Regardless of the diel shifting, temperatures in daytime and nighttime were stable. While relative humidity exhibited a reverse diel pattern to temperature, relative humidity was always greater than 95% in the gas chamber. During the entire experiment, the peat monolith experienced a range of atmospheric pressure from 100.18 kPa to 103.47 kPa. The averaged  $\text{CH}_4$  concentration in ambient air ( $C_{in}$ ) ranged from  $1.31 \text{ mg m}^{-3}$  to  $1.46 \text{ mg m}^{-3}$  (Fig. 3). While daytime  $C_{in}$  was relatively stable and consistent among the experimental weeks, nighttime  $C_{in}$  varied more, especially in the later period, with a maximum standard deviation of  $0.24 \text{ mg m}^{-3}$ .

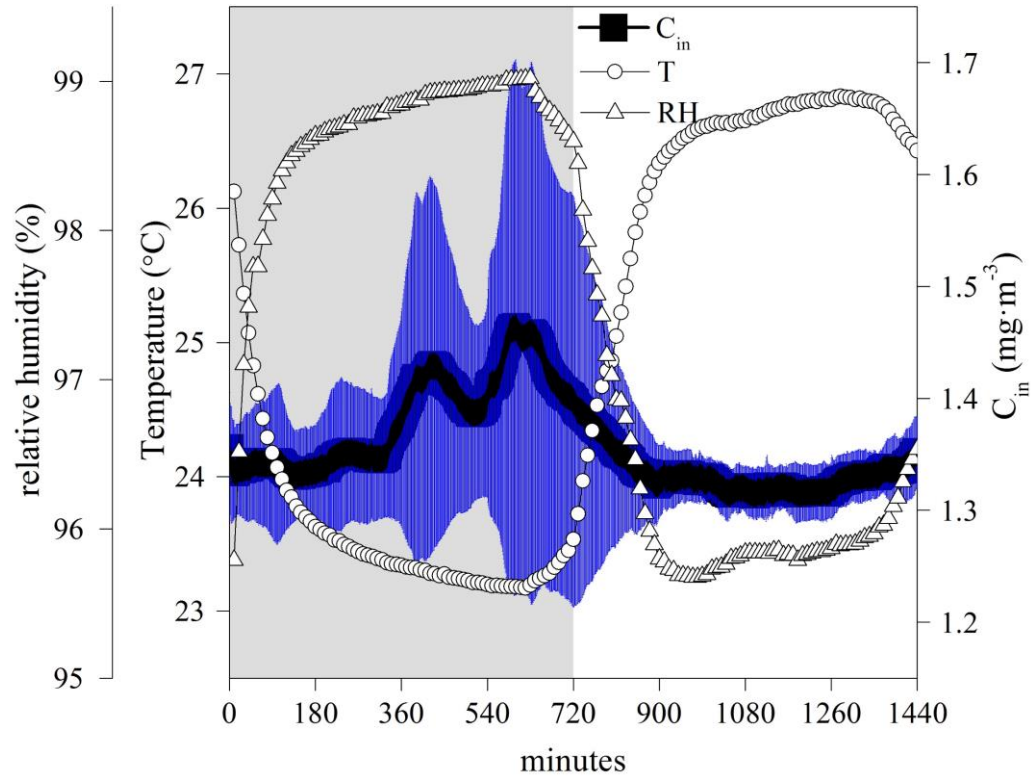


Figure 3 Averaged 10-minute temperature and relative humidity in gas chamber and averaged  $C_{in}$  for every minute. Standard deviation of  $C_{in}$  is shown by blue line. Shaded area denotes nighttime.

### 3.3. Gas content and dissolved $\text{CH}_4$ concentrations

Pre-incubation gas content for the upper, middle, and lower layers was  $0.04 \text{ m}^3 \text{ m}^{-3}$ ,  $0.06 \text{ m}^3 \text{ m}^{-3}$ , and  $0.07 \text{ m}^3 \text{ m}^{-3}$ , respectively. Gas content of middle and lower layers, ranging from  $0.06$  to  $0.14 \text{ m}^3 \text{ m}^{-3}$  and  $0.08$  to  $0.15 \text{ m}^3 \text{ m}^{-3}$ , respectively, generally increased from the start of the experiment with a higher rate of increase in week 1 to week 5 (Fig. 4A). The gas content of the upper layer, ranging from  $0.04$  to  $0.07 \text{ m}^3 \text{ m}^{-3}$ , showed a lower rate of increase throughout the experiment (Fig. 4A). The difference test indicated that gas content of the lower layer was significantly higher than the middle layer and the upper layer ( $P < 0.01$  in all comparisons).

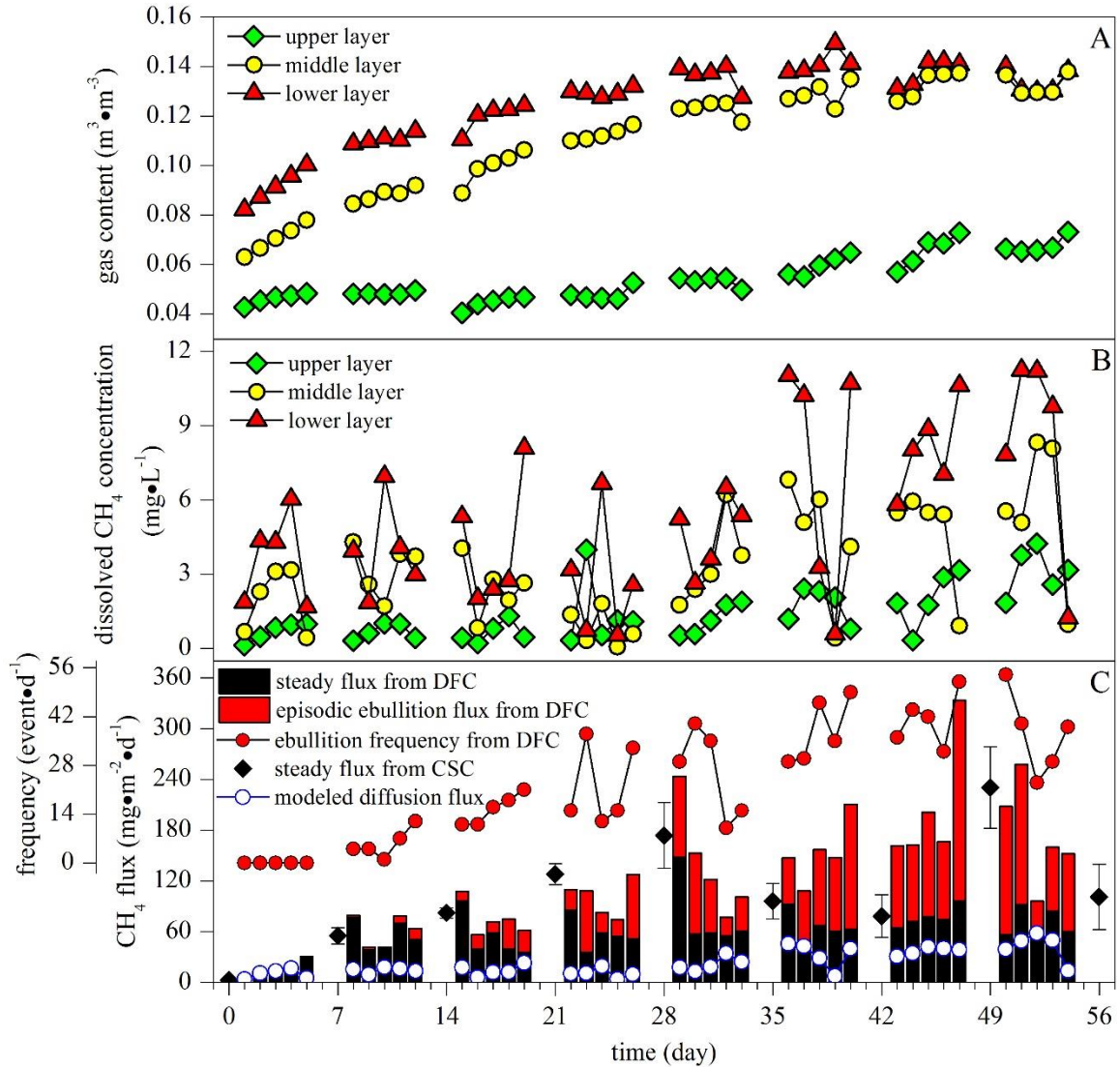


Figure 4 Gas content (A), dissolved  $\text{CH}_4$  concentrations (B), steady and ebullition fluxes, ebullition frequency, and modeled diffusion fluxes (C) for each day of the experiment.

Pre-incubation dissolved  $\text{CH}_4$  concentrations were  $0.075 \text{ mg L}^{-1}$ ,  $0.003 \text{ mg L}^{-1}$ , and  $0.007 \text{ mg L}^{-1}$ , respectively, for the upper, middle, and lower layers. Dissolved  $\text{CH}_4$  concentrations of the middle and lower layers increased rapidly after the experiment started but exhibited strong variability throughout the experiment with the largest concentration reduction ( $8.5 \text{ mg L}^{-1}$ ) in the lower layer (Fig. 4B). In contrast, dissolved

CH<sub>4</sub> concentrations of the upper layer increased slowly and smoothly (Fig. 4B). Despite the greater fluctuation in concentration, the lower layer of the monolith had significantly higher dissolved CH<sub>4</sub> concentrations (0.54 to 11.25 mg L<sup>-1</sup>) than the middle layer (0.07 to 8.33 mg L<sup>-1</sup>) and the upper layer (0.13 to 4.24 mg L<sup>-1</sup>) ( $P < 0.01$  in all comparisons). A positive correlation between dissolved CH<sub>4</sub> concentration and gas content was detected in the middle layer ( $R^2 = 0.40$ ,  $P < 0.05$ ) and upper layer ( $R^2 = 0.65$ ,  $P < 0.01$ ).

### 3.4. CH<sub>4</sub> fluxes measured using CSC

Twenty four out of 27 CSC flux measurements met the linearity criteria with  $R^2 > 0.90$  (Fig. A9). Pre-incubation CSC CH<sub>4</sub> flux was  $2.67 \pm 0.39$  mg m<sup>-2</sup> d<sup>-1</sup> (Fig. 4C).

Throughout the experiment, CSC CH<sub>4</sub> fluxes ranged from  $50.93 \pm 8.68$  mg m<sup>-2</sup> d<sup>-1</sup> to  $212.16 \pm 44.28$  mg m<sup>-2</sup> d<sup>-1</sup> with the highest flux observed in week 7 (Fig. 4C).

### 3.5. Modeled CH<sub>4</sub> diffusion fluxes

Modeled CH<sub>4</sub> diffusion fluxes from the peat monolith ranged from 3.48 mg m<sup>-2</sup> d<sup>-1</sup> to 53.43 mg m<sup>-2</sup> d<sup>-1</sup> (Fig. 4C). Modeled CH<sub>4</sub> diffusion fluxes had significant positive correlations with all measured gas content and dissolved CH<sub>4</sub> concentrations of the three layers ( $R^2$  ranging from 0.50 to 0.91;  $P < 0.01$  for all cases).

### 3.6. CH<sub>4</sub> fluxes measured using DFC

CH<sub>4</sub> fluxes measured by DFC and quantifications of steady fluxes and episodic ebullition fluxes are shown in Fig. A1-A8. The average uncertainty in DFC flux for the entire experiment was  $\pm 2.85\%$ . Steady fluxes (Fig. 4C), ranging from 3.84 mg m<sup>-2</sup> d<sup>-1</sup> to 148.05

$\text{mg m}^{-2} \text{ d}^{-1}$ , gradually increased in week 1 and then did not differ significantly after week 1 when compared on a weekly basis ( $P > 0.05$  for all comparisons). A difference test indicates that the steady fluxes from DFC were significantly higher than modeled  $\text{CH}_4$  diffusion fluxes ( $P < 0.01$ ). Episodic ebullition did not occur until the first day of week 2. Episodic ebullition fluxes, ranging from  $1.84 \text{ mg m}^{-2} \text{ d}^{-1}$  to  $237.31 \text{ mg m}^{-2} \text{ d}^{-1}$ , were then recorded, with fluxes generally increasing towards the end of the experiment. The highest daily ebullition flux occurred in the last day of week 7. Episodic ebullition fluxes for weeks 6, 7, and 8 were significantly higher than those for weeks 2, 3, and 4 ( $P < 0.01$  for all comparisons). After averaging steady fluxes and episodic ebullition fluxes measured within the same week and averaging CSC fluxes obtained before and after every experimental week, we found that steady fluxes from DFC were significantly lower than CSC fluxes ( $P < 0.05$ ) but CSC fluxes were not significantly different from total fluxes (steady plus episodic ebullition) from DFC ( $P > 0.05$ ). Ebullition frequency followed the same temporal pattern as ebullition fluxes ( $R^2 = 0.91$ ,  $P < 0.01$ ) with the first day of week 8 having the highest frequency of  $54 \text{ event d}^{-1}$ .

Figures 5A and 5C show the relationships between episodic ebullition fluxes, ebullition frequency and gas content of the three layers. Episodic ebullition fluxes increased dramatically when gas content of the middle and lower layers leveled off at  $0.14 \text{ m}^3 \text{ m}^{-3}$ . Relationships between ebullition frequency and gas content for either of these layers tended to be more linear. In contrast, positive but weak relationships exist between dissolved  $\text{CH}_4$  concentrations and episodic ebullition flux and frequency for the upper and lower layers (Fig. 5B and D).

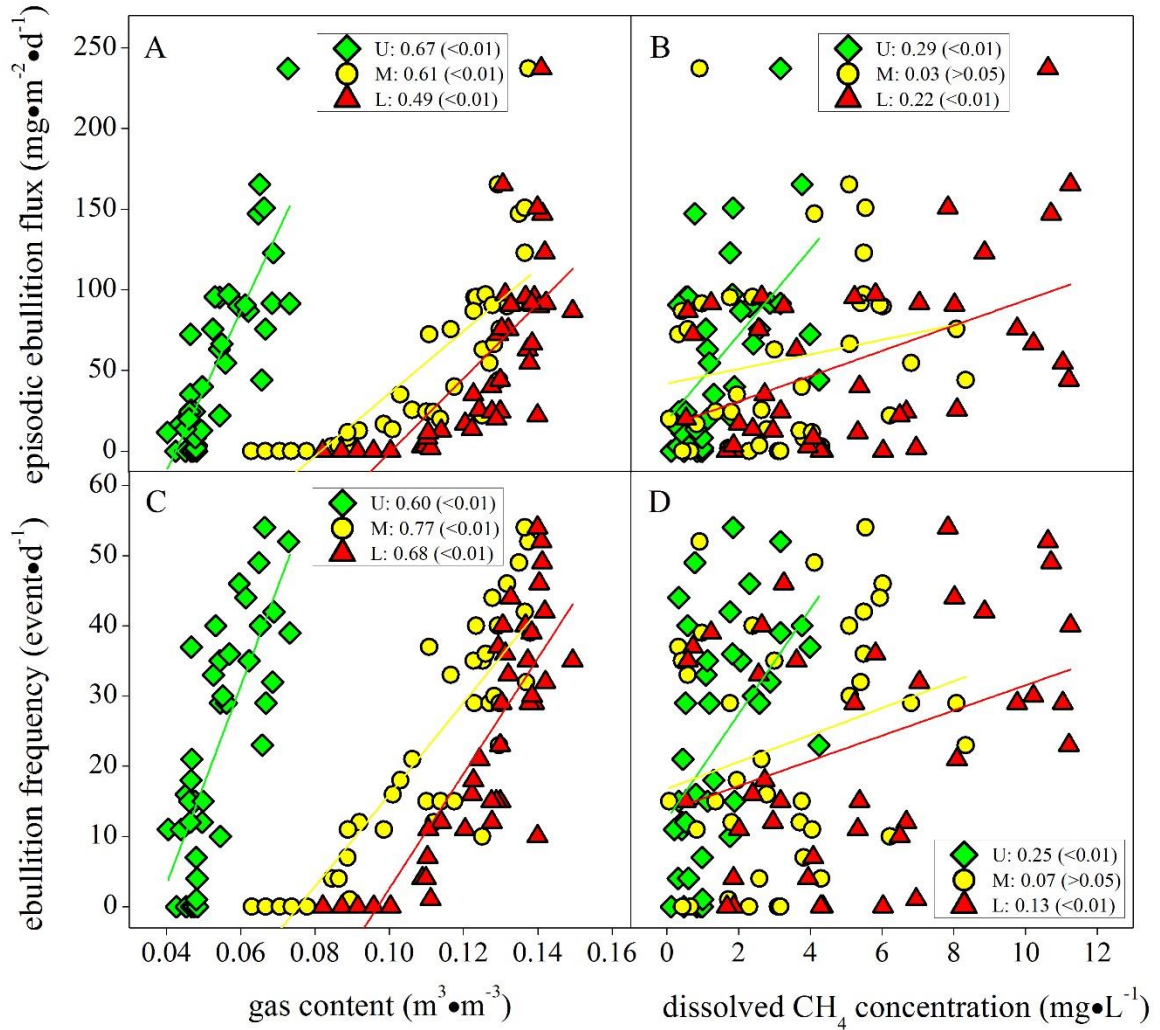


Figure 5 Relationships between gas content, dissolved CH<sub>4</sub> concentrations, ebullition fluxes, and ebullition frequency for three layers. Letter 'U', 'M', and 'L' in the figure represent upper, middle, and lower layers, respectively. Linear regression lines are shown. R<sup>2</sup> and P values of the linear regressions are shown in the legend and in bracket, respectively.

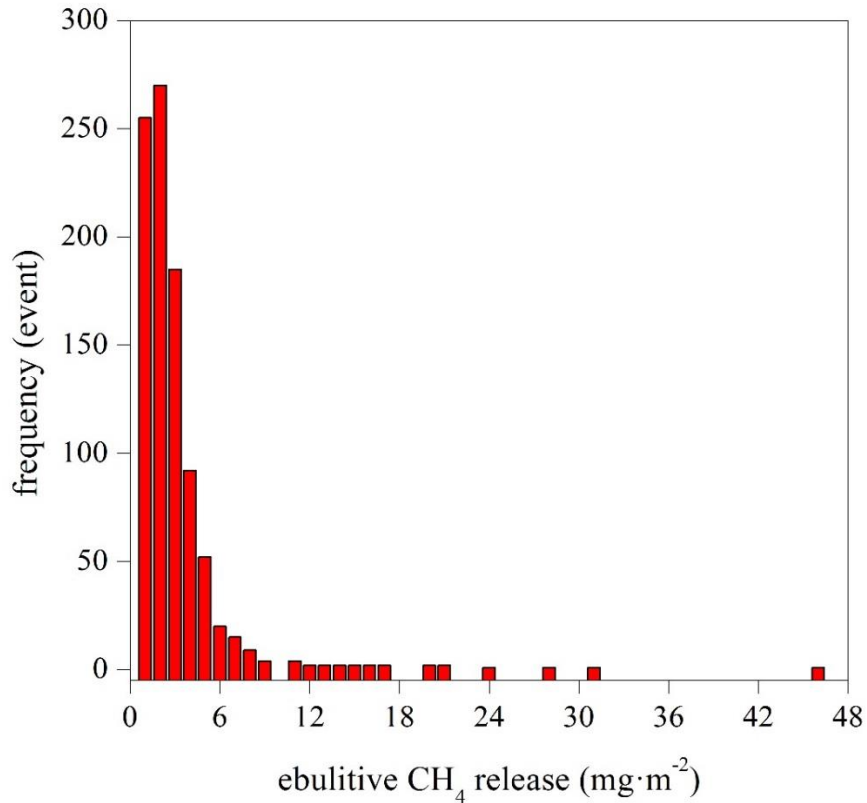


Figure 6 Frequency distribution of ebullition CH<sub>4</sub> releases observed over the entire study period (n=926).

There were in total 926 events of ebullitive CH<sub>4</sub> release, ranging from 0.12 mg m<sup>-2</sup> to 45.86 mg m<sup>-2</sup>, observed in this study. The frequency distribution of ebullitive CH<sub>4</sub> releases was non-normal with a strong positive skew (Fig. 6), with 95% of ebullitive CH<sub>4</sub> releases being below 6.12 mg m<sup>-2</sup>. A negative coupling between atmospheric pressure and ebullitive CH<sub>4</sub> releases is evident from plotting the time series of both parameters together (Fig. 7). Ebullition occurred more frequently in daytime than in nighttime over the entire experiment ( $P < 0.01$ ) (Fig. 8A and B). While the ebullitive CH<sub>4</sub> flux was not significantly different between daytime and nighttime for week 2 to week 5 ( $P > 0.05$ ), larger ebullitive CH<sub>4</sub> releases occurred during nighttime when temperature was lower for

week 6 to week 8 ( $P<0.01$ ) (Fig. 8A and B). The cumulative ebullitive  $\text{CH}_4$  releases and the frequency of ebullition, both calculated for every 12 hours in each experimental day, were significantly and negatively related to changes in atmospheric pressure, defined as the difference between averaged atmospheric pressure for any 12-hours and that of the previous 12-hours, especially in week 6 to week 8 ( $P<0.01$  for all cases) (Fig. 8C and D).

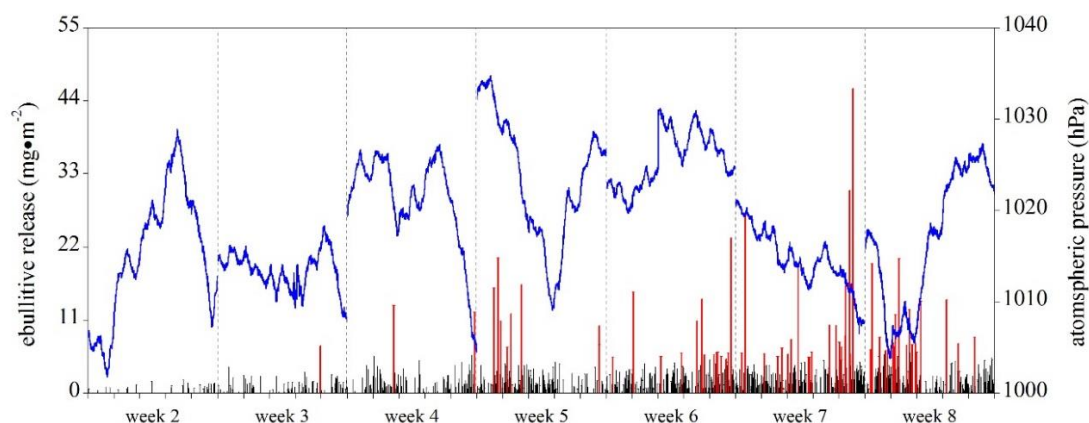


Figure 7 Ebullitive  $\text{CH}_4$  releases and atmospheric pressure as a function of time. The largest 5% of ebullition  $\text{CH}_4$  releases are shown in red.

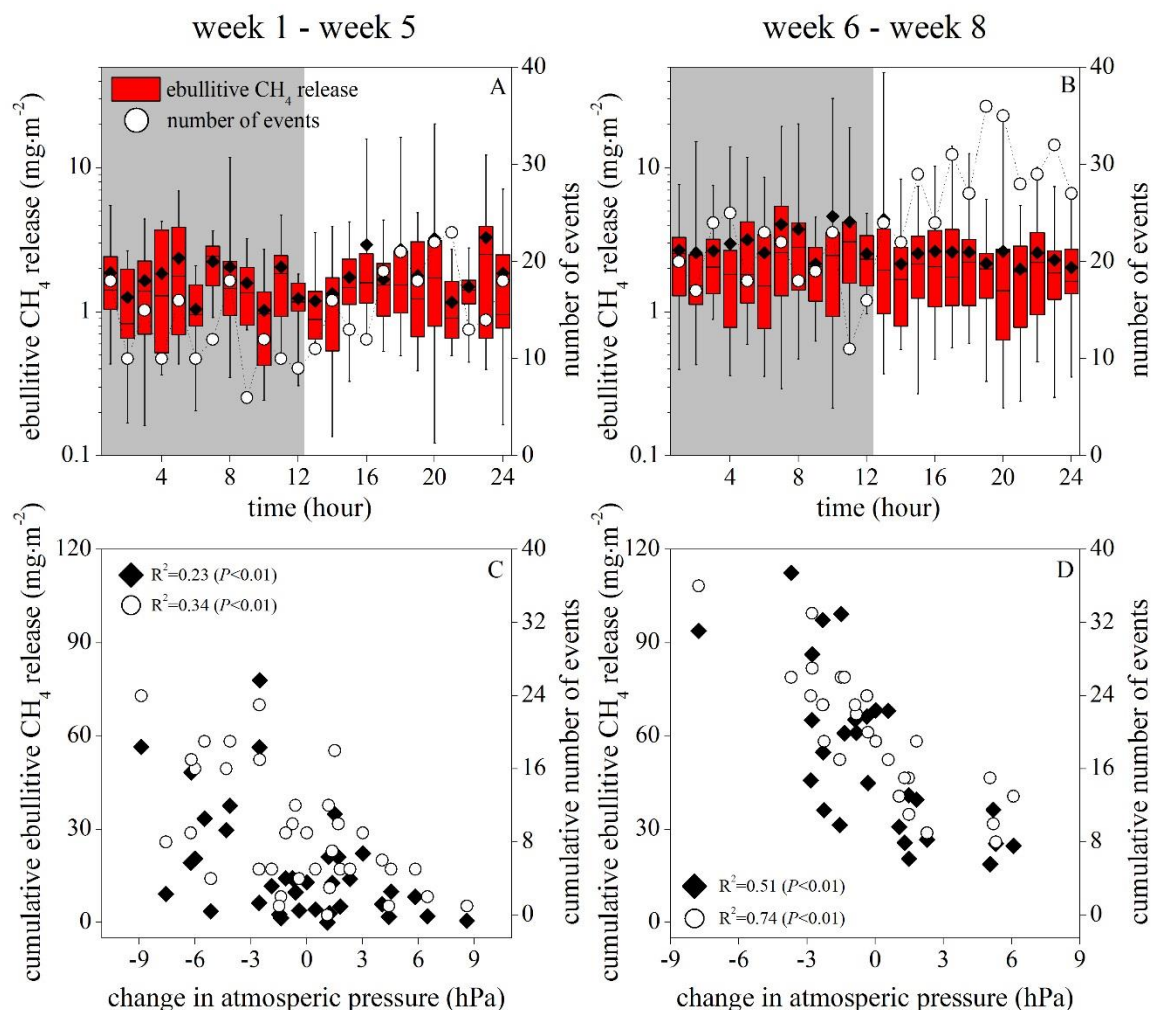


Figure 8 (A) and (B) ebullitive  $\text{CH}_4$  releases observed every experimental hour for weeks 2-5 and weeks 6-8, respectively. The box shows the distance between the 25<sup>th</sup> and 75<sup>th</sup> percentiles, with the 50<sup>th</sup> percentile shown as a line. The error bars denote the minimum and maximum, and the filled diamond denotes the average. Note log scale for y axis. (C) and (D) relationships between cumulative ebullitive  $\text{CH}_4$  release (filled diamond), cumulative number of ebullition (open cycle) and change in atmospheric pressure for weeks 2-5 and weeks 6-8, respectively. Linear regression  $R^2$  and  $P$  values are shown.

## 4. Discussion

### 4.1. Reliability of DFC for continuously monitoring CH<sub>4</sub> ebullition

Using the graphical model adopted here, the quantification of episodic ebullition fluxes depends critically on the choice of the baseline. Unfortunately, the accumulation of ebullition-derived CH<sub>4</sub> in the gas chamber is a shortcoming of the DFC system as it is superimposed on the steady fluxes and thus complicates the baseline identification in the flux graphs. The steady baseline can be accurately defined when episodic ebullition is infrequent, but we have to assume a trend for the steady fluxes when the baseline is obscured by the ebullition peaks (Fig. 2B). We assume that higher ebullition frequency results in higher uncertainty in defining the baseline. We assigned an arbitrary error level, ranging from  $\pm 1\%$  to  $\pm 10\%$ , proportional to the ebullition frequency, to the steady fluxes and propagated this error to the resulting episodic ebullition fluxes. As shown in Fig. 9, when ebullition frequency was higher than 27 event d<sup>-1</sup> and calculated episodic ebullition fluxes constituted over half of the total flux, the distribution of potential error in calculated episodic ebullition fluxes is constrained to a very narrow range, highlighting the insensitivity of episodic ebullition fluxes to the quantification of the steady fluxes during the later phase of the experiment.

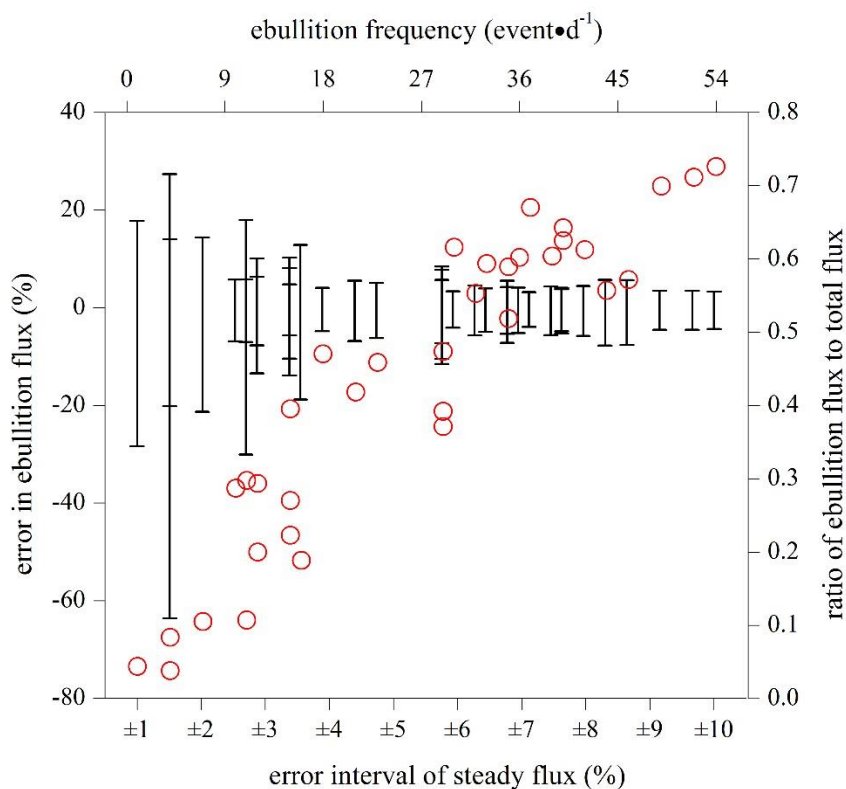


Fig. 9 Propagated error in calculated episodic ebullition fluxes using the graphical model (error bars) and relationship between ebullition frequency and the ratio of ebullition flux to total flux (red dots).

It may be argued that the natural  $\text{CH}_4$  gradient at the air-peat interface was reduced by long-term closure of the gas chamber and excess accumulation of ebullition-derived  $\text{CH}_4$  such that the natural regime of steady emission was disturbed [Hutchinson et al., 2000]. Averaged bulk  $\text{CH}_4$  concentration of the peat monolith calculated by Eq. 8 (2.26 to 33.76  $\text{mg L}^{-1}$ ) was at least three orders higher than dissolved  $\text{CH}_4$  concentration (0.04 to 1.13  $\mu\text{g L}^{-1}$ ) equilibrating with observed  $C_{out}$  (1.32 to 35.43  $\mu\text{g L}^{-1}$ ). In contrast to other types of soil, the combination of high porosity and essentially unlimited biogenic  $\text{CH}_4$  production potential in peat results in a large  $\text{CH}_4$  reservoir and high ebullition potential

for peat. As a result, given the relatively high purging flow rate applied in this study, the disturbance of the natural gas exchange regime was minimal during the DFC measurements, and the smooth change of steady fluxes under ebullition peaks can be justified in the graphical model.

When compared on a weekly basis, steady fluxes measured by DFC were significantly lower than fluxes from CFC ( $P < 0.05$ ) but significantly higher than modeled diffusion fluxes ( $P < 0.01$ ) (Fig. 4C). Due to the dominance of *Sphagnum* species, we can safely assume that plant-mediated  $\text{CH}_4$  transport was negligible in this peat monolith [Stephen et al., 1998b]. Subsequently, the differences between fluxes estimated from these three methods is most likely attributed to steady ebullition from the peat. Coulthard et al. [2009] proposed that shallow peat layers are sources of steady  $\text{CH}_4$  ebullition that is released to the atmosphere as a continuous stream of relatively small bubbles, causing a linear increase of the  $\text{CH}_4$  concentration in CSC headspace over time. However, the large differences in temporal resolution between CSC and DFC make it difficult to extract valuable information from the comparison of their results. While CSC measurements span 90 minutes for every experimental week, continuous DFC monitoring, which accounts for considerable temporal variability in the dissolved  $\text{CH}_4$  reservoir in peat (Fig. 4B), provides a better characterization of temporal variability in  $\text{CH}_4$  diffusion fluxes. In the later phase of our experiment, we observed much larger deviation in the replicate CSC measurements (Fig. 4C and A9). It is possible that the observed high CSC fluxes (e.g., those measured after week 4, week 7, and week 8, Fig. 4C and A9) might include time periods of active steady ebullition. After using the lowest values of replicate

measurements only to re-calculate CSC fluxes after week 4, week 7, and week 8, no significant difference was found between CSC fluxes and steady fluxes from DFC ( $P>0.05$ ).

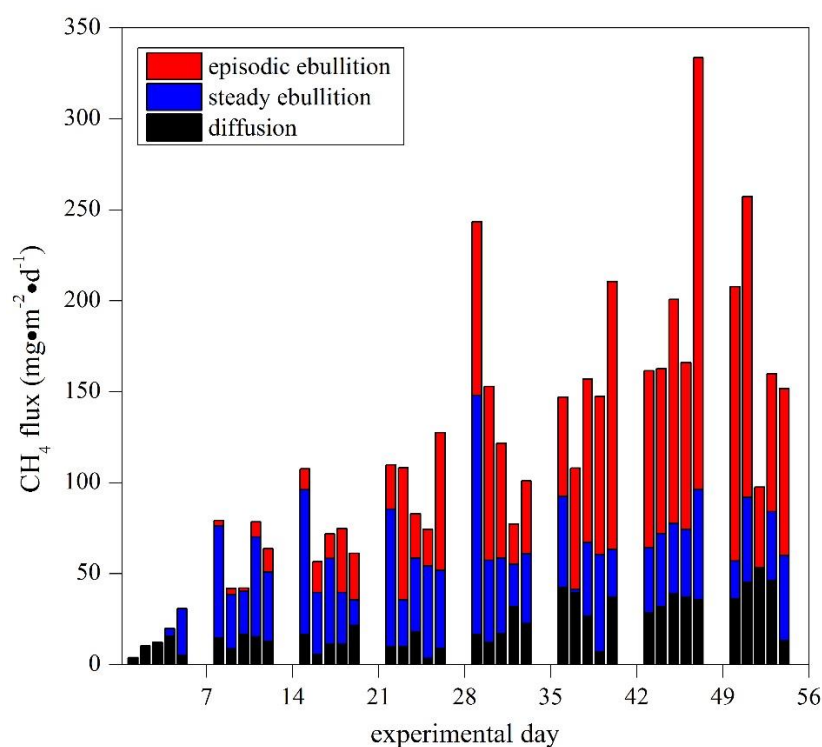


Fig. 10 Partitioned diffusion flux, steady ebullition flux, and episodic ebullition flux for each experimental day.

Therefore, we calculated the steady ebullition fluxes as the difference between steady fluxes from DFC and modeled diffusion fluxes (Fig. 10). Episodic ebullition constituted 0 to 72% of the total fluxes with an average of 38% throughout the experiment, being consistent with previous findings of 17% ~ 52% using similar flow-through systems at the same scale [Christensen et al., 2003]. Steady ebullition constituted 0 to 83% of the total fluxes with an average of 36%. To our knowledge, this is the first attempt to

quantify steady ebullition fluxes from peat. However, the definition of steady ebullition may depend on the detection sensitivity of measurement systems. Assuming that the mixing ratio of CH<sub>4</sub> to the total gases in a bubble is 0.2 [Tokida et al., 2007], the lowest observed ebullitive CH<sub>4</sub> release, 0.12 mg m<sup>-2</sup>, suggests that a released gas bubble with volume smaller than ~0.08 cm<sup>3</sup> may be classified as steady ebullition under the typical incubation conditions of this experiment. Moreover, with a single FMA we were unable to separate the potential contribution of fluctuations in  $C_{in}$  to the variations of measured steady fluxes (Fig. 3). However, this limitation could be easily fixed in a future study with better constraints on  $C_{in}$  dynamics.

We argue that the DFC implemented in a long-term chamber closure is a potentially superior technique to other conventional methods for continuous CH<sub>4</sub> ebullition monitoring in peat. In many cases, the underlying mechanical processes in the peat matrix may be independent of the respective ambient or chamber CH<sub>4</sub> concentrations, plant physiology, and turbulence conditions of the chamber headspace [Mastepanov and Christensen, 2009]. Furthermore, all CH<sub>4</sub> exchange from the isolated monolith can be directly measured by DFC for months without any missing ebullition events. Given the high temporal resolution of DFC, individual ebullition events can be explicitly identified even on a short time scale. Within combination with additional constraints on diffusion and plant-dependent emissions, the DFC system has the potential to precisely partition pathways of CH<sub>4</sub> emissions from peat soils.

#### **4.2. Couplings between CH<sub>4</sub> ebullition and subsurface CH<sub>4</sub> dynamics**

Previous laboratory studies have found that even under careful wetting procedures initial under-saturation occurred in undisturbed peat samples, such that the initial gas content was ranged from 0.01 to 0.13 m<sup>3</sup> m<sup>-3</sup> [Beckwith and Baird, 2001; Baird et al., 2004; Strack et al., 2005]. In our study initial gas contents ranged from 0.04 to 0.07 m<sup>3</sup> m<sup>-3</sup> for the three layers, and fast rates of gas buildup were observed before the first ebullition in week two, especially for the middle and lower layers (Fig. 4A). Although the time to the initiation of ebullition (10 days) was shorter than measured in other studies [e.g., Baird et al., 2004] due possibly to the higher incubation temperature of this study, the gas contents at the first ebullition, 0.05 to 0.11 m<sup>3</sup> m<sup>-3</sup>, and maximum gas contents, 0.07 to 0.15 m<sup>3</sup> m<sup>-3</sup>, are consistent with the range reported in previous studies [Baird et al., 2004; Strack et al., 2005; Kellner et al., 2006]. We also found that the dissolved CH<sub>4</sub> concentrations in pore water during gas buildup and initial ebullition were below the theoretical equilibrium concentration (~8 mg L<sup>-1</sup>) previously assumed necessary for bubble formation (Fig. 4B) [Baird et al., 2004]. Recently, Laing et al. [2008], using membrane inlet quadrupole mass spectrometry, found an average dissolved CH<sub>4</sub> concentration of 1.3 mg L<sup>-1</sup> to be equilibrated with gas bubbles comprising 11% by volume in shallow peat samples. Together with others, our findings support the argument that peatland CH<sub>4</sub> models only using nucleation to predict gas buildup and ebullition are likely to need revision because minute gas bubbles are always present in the peat pore space [Baird et al., 2004; Strack et al., 2005], causing a lowered equilibrium concentration for the dissolved phase and serving as initial nuclei for biogenic bubble growth [Waddington et al., 2009]. Without taking gas bubble dynamics into account, peatland models tend to

underestimate ebullition fluxes by assuming a high dissolved CH<sub>4</sub> concentration for ebullition initiation [Baird et al., 2004].

In a field study in a near-surface fen peat, Strack et al. [2005] reported positive relationships between dissolved CH<sub>4</sub> concentrations and bubble fluxes at different peat depth, and it has also been shown that large reductions in dissolved CH<sub>4</sub> concentrations can occur during short time periods of active ebullition [Strack and Waddington, 2008].

In this study dissolved CH<sub>4</sub> concentrations correlate to gas contents positively and significantly in the upper layer ( $R^2=0.65$ ,  $P<0.01$ ), but no significant correlation was detected in the middle and lower layers where gas contents were consistently larger ( $P>0.05$ ). Moreover, dissolved CH<sub>4</sub> concentrations resolved limited variations in episodic ebullition fluxes and frequency (Fig. 5C and D). Several factors may explain the generally decoupled relationship between dissolved CH<sub>4</sub> concentrations and gas contents and episodic ebullition. One possibility is that dissolved CH<sub>4</sub> concentrations are highly variable spatially within the peat and at scales much smaller than the pore-water samplers [Baird et al., 2004; Reid et al., 2013]. Consequently, the measured dissolved CH<sub>4</sub> concentrations might be subject to the micro-environment in the immediate vicinity of the pore-water samplers [Waddington et al., 2009]. Such scaling problems may also exist in field studies using spatially discrete sampling methods. More importantly, due to its low solubility, CH<sub>4</sub> is predominantly stored in gaseous form even when a small bubble volume is present in the peat [Strack and Waddington, 2008]. The disproportion in subsurface CH<sub>4</sub> stocks implies that: Dissolved CH<sub>4</sub> concentrations may be regulated by the storage and release of gas bubbles, resulting in dramatic changes in concentration

during the main period of ebullition (Fig. 4C). Another possibility is that CH<sub>4</sub> bubbles can be produced directly by granular microbial consortia containing methanogens such that dissolved CH<sub>4</sub> concentration is controlled by bubbles going into solution [Green and Baird, 2012]. Based on our observations, we suggest that gas bubble dynamics in near-surface peat may be decoupled from the dissolved CH<sub>4</sub> pool and the physical characteristics of peat alone can then be important in determining ebullition fluxes [Laing et al., 2008].

As first proposed by Baird et al. [2004], peat soils may need to exceed a threshold bubble volume before ebullition can occur. In an effort to model ebullition based on this threshold theory, Kellner et al. [2006] further suggested a fuzzy threshold, rather than a single value, related to intrinsic properties of peat-bubble interactions, is responsible for the complex ebullition behavior of peat. Despite its conceptual simplicity [Coulthard et al., 2009], the threshold theory has proven to be effective in several laboratory [Comas and Slater, 2007; Slater et al., 2007] and field [Strack et al., 2005] studies with resolved threshold gas content ranging from 0.07 to 0.16 m<sup>3</sup> m<sup>-3</sup> for poorly-decomposed near-surface *Sphagnum* peat. In our study, distinct differences in gas content and rate of gas bubble buildup among three layers were resolved (Fig. 4A). While all three layers showed a significant linear relationship between gas content and ebullition fluxes, ebullition fluxes increased dramatically after the gas content of middle and lower layers leveled off at 0.14 (Fig. 5A), an observation consistent with threshold-based ebullition. Thus, our work supports threshold theory using directly measured episodic CH<sub>4</sub> ebullition fluxes. More importantly, different relationships between gas content and episodic

ebullition fluxes found in the three layers highlight the role that vertical heterogeneity of peat structure may have on gas bubble dynamics even in this very shallow peat monolith.

The physical properties of peat, including the porosity, bulk density, decomposition degree, pore size distribution, and compressibility, exert a strong control on peatland ecohydrology and biogeochemistry [Price et al., 2005]. Recently, geophysical imaging methods have been employed to better understand how the physical structure of peat entraps gas bubbles. By using X-ray computed tomography, Kettridge and Binley [2011] concluded that the compressibility and the ability of *Sphagnum* peat to trap biogenic gas bubbles depends not only on the bulk volume of the peat constituents, which is usually inferred from the bulk density and porosity, but also on their spatial arrangement within the peat. The presence of longer structural components, like stems and branches, strongly increases the tortuosity of pore networks and the ability of peat to trap bubbles. In a laboratory study using electrical resistivity, Slater et al. [2007] revealed that biogenic gas bubbles tend to accumulate at certain depths (within 0.04 to 0.10 m below the water table in their case) within the shallow *Sphagnum* peat as thin layers due to the prevalently layered nature of peat. Based on such findings, differences in gas content and the relationship between gas content and episodic ebullition fluxes among three layers in our peat monolith may be attributed to layered structural differences in peat. The compressibility of peat decreases with increasing decomposition degree [Price et al., 2005]. As peat decomposes with depth, plant remnants successively adjust from a disordered to a layered firmer framework [Boelter, 1969]. In this study, more decomposed middle and lower layers with the presence of rigid root fibers and wood

inclusions had higher bulk densities than the upper layer and may have a denser and more tortuous pore networks to entrap gas bubbles [Kettridge and Binley, 2011]. On the other hand, decreased compaction near the peat surface together with the absence of rigid structural components may make the upper layer less resistant to bubble release [Comas and Slater, 2007].

Interestingly, ebullition frequency increased linearly with gas content and did not exhibit a threshold effect (Fig. 5B). Given that dissolved  $\text{CH}_4$  concentrations measured from the three layers were always supersaturated against the chamber air (Fig. 4B), it is reasonable to speculate that the enhanced episodic ebullition in the last three weeks (Fig. 7) is attributed to the less frequent releases of large gas bubbles, rather than depth-independent releases of bubbles with more concentrated  $\text{CH}_4$ . While the upper layer with a lower bubble trapping potential might have a fast “bubble turnover” and be the source of small episodic ebullition events, large gas bubbles might be episodically vented from the middle and lower layers once the high ebullition threshold was reached. Therefore, we argued that the latest peatland  $\text{CH}_4$  models applying a single ebullition threshold for the entire depth of peat [e.g., Zhang et al., 2012] may not be able to resolve the complex spatiotemporal pattern of  $\text{CH}_4$  ebullition. Similarly, models adopting the pressure balance criteria to predict ebullition [e.g., Tang et al., 2010] may fail to capture large ebullition events originating from deep peat layers where the bubble trapping potential is much higher and over-pressurized stratum are formed. We propose that a depth-dependent multi-threshold model determined by peat physical structure should be adopted in  $\text{CH}_4$  models as the criteria for ebullition prediction.

### 4.3. Relative importance of atmospheric pressure and temperature as ebullition trigger

Both atmospheric pressure and temperature have been identified as ebullition triggers (Table 1). In this study, the incubation temperatures (23 °C ~ 27 °C) were much higher than the peat monolith studied would experience naturally on an annual basis. Optimal temperatures for CH<sub>4</sub> production have been found to be between 10 °C and 12 °C for northern peat samples [Williams and Crawford, 1984]. Bergman et al. [1998] suggested that high-temperature incubations (above 20 °C in their case) of *Sphagnum* peat tend to decouple CH<sub>4</sub> production from temperature. In this sense, a temperature higher than the optimal range for CH<sub>4</sub> production is desirable to minimize its biological control on CH<sub>4</sub> ebullition. On the other hand, an approximately 4 °C fluctuation in the diel cycle (Fig. 3), theoretically identical to a 40 hPa change in atmospheric pressure in terms of driving bubble volume alteration [Tokida et al., 2009], is sufficiently large to assess the triggering effects of temperature.

In week 2 to week 5, ebullitive CH<sub>4</sub> releases had no significant difference between daytime and nighttime (Fig. 8A), and ebullition fluxes were not coincide with changes in atmospheric pressure (Fig. 8C), indicating that both changes in temperature and atmospheric pressure had limited controls on CH<sub>4</sub> ebullition when gas contents were far below the ebullition thresholds. When the bubble buildup in the middle and lower layers was substantial in week 6 to week 8, the ebullition frequency increased greatly in the daytime (Fig. 8B). If the increased daytime temperature was able to trigger episodic ebullition from the middle and lower layers during this time period, we would expect to

see outliers of ebullitive CH<sub>4</sub> releases, illustrated by the length of upper error bars for every experimental hour in Fig. 8B, during daytime. In fact, however, those outliers tended to occur in nighttime (Fig. 8B) and were often found to be coupled with large drops in atmospheric pressure (Fig. 7). Due to the highly skewed frequency distribution of ebullitive CH<sub>4</sub> releases, those large CH<sub>4</sub> ebullition events might dominate the time-integrative ebullition fluxes (Fig. 6). Therefore, the negative linear relationship between cumulative ebullitive CH<sub>4</sub> releases and changes in atmospheric pressure with largely improved significance in week 6 to week 8 (Fig. 8D) further suggests that atmospheric pressure was responsible for triggering large CH<sub>4</sub> ebullition from deeper layers where big bubbles were trapped.

The effectiveness of temperature changes in triggering ebullition may result from the thermal conductivity of peat [Yoshikawa et al., 2009]. Previous studies have illustrated that the thermal conductivity of peat decreases with water content and decomposition degree [O'Donnell, 2009]. In our study, the unsaturated moss layer in the upper 2 cm might insulate the deeper layers from warm air in daytime. In addition, even below the water table, poorly decomposed surface peat might also dampen the amplitude of downward heat flux to a large degree [Yoshikawa et al., 2009]. Although we do not have enough information on the temperature dynamics of deeper layers, as implied by other studies [e.g., Tokida et al., 2007] the diel temperature cycle in the middle and lower layers might be small. Therefore, we speculated that the triggering effects of temperature were mostly limited to the upper layer where a low ebullition threshold existed, which resulted in small and frequent ebullitive CH<sub>4</sub> releases observed in daytime (Fig. 8B).

On the other hand, since the pressure of a gas bubble below the water table is always the sum of hydrostatic and atmospheric pressures, changes in atmospheric pressure influence the volume of the gas bubble trapped throughout peat profiles in a more direct manner. Moreover, the alteration of gas bubble caused by changes in atmospheric pressure occurs almost instantly, giving the CH<sub>4</sub> ebullition an episodic nature. While increasing atmospheric pressure was also found to facilitate small ebullition events from upper layers of the peat by allowing size-reduced gas bubbles to pass through fiber networks [Comas and Wright, 2012], our data suggests that large ebullition events originating from deeper layers are triggered by drops in atmospheric pressure in peat soils.

## 5. Conclusions

In this study, we successfully demonstrated the capability of DFC for continuously monitoring CH<sub>4</sub> ebullition from a near-surface *Sphagnum* peat and its potential to partition the pathways of CH<sub>4</sub> emission. The application of DFC with coupled subsurface gas content and dissolved CH<sub>4</sub> concentration measurements at laboratory scale offers new opportunities for understanding the complex behavior of CH<sub>4</sub> ebullition and its couplings to subsurface gas bubble dynamics. Our work highlights a need to integrate peat physical structure into ebullition models. The structural heterogeneity of peat gives rise to a depth-dependent multi-threshold model that was responsible for the spatiotemporal variation of CH<sub>4</sub> ebullition and partially determines the relative importance of changes in atmospheric pressure and temperature in triggering ebullitive CH<sub>4</sub> releases. Future efforts should be dedicated to applying the DFC technique at the field scale to better improve our knowledge of CH<sub>4</sub> ebullition in northern peatlands.

## References

- Baird, A., C. W. Beckwith, S. Waldron, J. M. Waddington (2004), Ebullition of methane-containing gas bubbles from near-surface *Sphagnum* peat, *Geophys. Res. Lett.*, *31*, L21505.
- Beckwith, C. W. and A. J. Baird (2001), Effect of biogenic gas bubbles on water flow through poorly decomposed blanket peat, *Water Resour. Res.*, *37*(3), 551-558.
- Bergman, I., B. H. Svensson, M. Nilsson (1998), Regulation of methane production in a Swedish acid mire by pH, temperature and substrate, *Soil Biol. Biochem.*, *30*(6), 729-741.
- Boelter, D. H. (1969), Physical properties of peat as related to degree of decomposition, *Soil Sci. Soc. Am. J.*, *33*, 606-609.
- Bragazza, L., J. Parisod, A. Buttler, R. D. Bardgett (2012), Biogeochemical plant-soil microbe feedback in response to climate warming in peatlands. *Nat. Clim. Chang.*, *3*(3), 273-277.
- Bridgham, S. D., H. Cadillo-Quiroz, J. K. Keller, Q. Zhuang (2013), Methane emissions from wetlands: biogeochemical, microbial, and modeling perspectives from local to global scales. *Glob. Chang. Biol.*, doi: 10.1111/gcb.12131.
- Christensen, T. R., N. Panikov, M. Mastepanov *et al.* (2003), Biotic controls on CO<sub>2</sub> and CH<sub>4</sub> exchange in wetlands – a closed environment study, *Biogeochemistry*, *64*, 337-354.
- Comas, X. and L. Slater (2007), Evolution of biogenic gases in peat blocks inferred from noninvasive dielectric permittivity measurements, *Water Resour. Res.*, *43*, W05424.
- Comas, X., L. Slater, A. Reeve (2007), In situ monitoring of free-phase gas accumulation and release in peatlands using ground penetrating radar (GPR), *Geophys. Res. Lett.*, *34*, L06402.
- Comas, X., L. Slater, A. Reeve (2008), Seasonal geophysical monitoring of biogenic gases in a northern peatland: Implications for temporal and spatial variability in free phase gas production rates, *J. Geophys. Res.*, *113*, G01012.
- Comas, X. and W. Wright (2012), Heterogeneity of biogenic gas ebullition in subtropical peat soils is revealed using time-lapse cameras, *Water Resour. Res.*, *48*, W04601.
- Coulthard, T. J., A. J. Baird, J. Ramirez, J. M. Waddington (2009), Methane dynamics in peat: Importance of shallow peats and a novel reduced-complexity approach for modeling ebullition. In: Baird, A., L. Belyea, X. Comas, A. Reeve, L. Slater (eds) *Northern peatlands and carbon cycling*, AGU, Washington, 173-185

- Fechner-Levy, E. J., and H. F. Hemond (1996), Trapped methane volume and potential effects on methane ebullition in a northern peatland, *Limnol. Oceanogr.*, *41*(7), 1375-1383.
- Glaser, P. H., J. P. Chanton, P. Morin, D. O. Rosenberry, D. I. Siegel, O. Ruud, L. I. Chasar, A. S. Reeve (2004), Surface deformations as indicators of deep ebullition fluxes in a large northern peatland, *Glob. Biogeochem. Cycles*, *18*, GB1003.
- Goodrich, J. P., R. K. Varner, S. Frolking, B. N. Duncan, P. M. Crill (2011), High-frequency measurements of methane ebullition over a growing season at a temperate peatland site, *Geophys. Res. Lett.*, *38*, L07404.
- Green, S. M. and A. J. Baird (2012), A mesocosm study of the role of the sedge *Eriophorum angustifolium* in the efflux of methane – including that due to episodic ebullition – from peatlands, *Plant Soil*, *351*, 207-218.
- Hutchinson, G. L., G. P. Livingston, R. W. Healy, R. G. Striegl (2000), Chamber measurement of surface-atmosphere trace gas exchange: Numerical evaluation of dependence on soil, interfacial layer, and source/sink properties, *J. Geophys. Res.*, *105*(D7).
- Kellner, E., J. M. Waddington, J. S. Price (2005), Dynamics of biogenic gas bubbles in peat: Potential effects on water storage and peat deformation, *Water Resour. Res.*, *41*, W08417.
- Kellner, E., A. J. Baird, M. Oosterwoud, K. Harrison, J. M. Waddington (2006), Effect of temperature and atmospheric pressure on methane (CH<sub>4</sub>) ebullition from near-surface peats, *Geophys. Res. Lett.*, *33*, L18405.
- Kettridge, N. and A. Binley (2011), Characterization of peat structure using X-ray computed tomography and its control on the ebullition of biogenic gas bubbles, *J. Geophys. Res.*, *116*, G01024.
- Lai, D. Y. F. (2009), Methane dynamics in northern peatlands: a review, *Pedosphere*, *19*(4), 409-421.
- Lai, D. Y. F., N. T. Roulet, E. R. Humphreys, T. R. Moore, M. Dalva (2012), The effect of atmospheric turbulence and chamber deployment period on autochamber CO<sub>2</sub> and CH<sub>4</sub> flux measurements in an ombrotrophic peatland, *Biogeosciences*, *9*, 3305-3322.
- Laing, C. G., T. G. Shreeve, D. M. E. Pearce (2008), Methane bubbles in surface peat cores: *in situ* measurements, *Glob. Chang. Biol.*, *14*, 916-924.
- Mastepanov, M. and T. R. Christensen (2009), Laboratory investigations of methane buildup in, and release from, shallow peats. In: Baird, A., L. Belyea, X. Comas, A.

- Reeve, L. Slater (eds) *Northern peatlands and carbon cycling*, AGU, Washington, 205-218.
- McDermitt, D., G. Burba, L. Xu et al. (2011), A new low-power, open-path instrument for measuring methane flux by eddy covariance, *Appl. Phys. B*, *102*, 391-405.
- Nielson, K. K., V. C. Rogers, G. W. Gee (1984), Diffusion of radon through soils: A pore distribution model, *Soil Sci. Soc. Am. J.*, *48*(3), 482-487.
- Oswald, R., T. Behrendt, M. Ermel et al. (2013), HONO emissions from soil bacteria as a major source of atmospheric reactive nitrogen, *Science*, *341*, 1233.
- O'Donnell, J. A., V. E. Romanovsky, J. W. Harden, A. D. McGuire (2009), The effect of moisture content on the thermal conductivity of moss and organic soil horizons from black spruce ecosystems in interior Alaska, *Soil Sci.*, *174*(12), 646-651.
- Panikov, N. S., M. A. Mastepanov, T. R. Christensen (2007), Membrane probe array: Technique development and observation of CO<sub>2</sub> and CH<sub>4</sub> diurnal oscillations in peat profile, *Soil Biol. & Biochem.*, *39*(7), 1712-1723.
- Pape, L., C. Ammann, A. Nyfeler-Brunner, C. Spirig, K. Hens, F. X. Meixner (2009), An automated dynamic chamber system for surface exchange measurement of non-reactive and reactive trace gases of grassland ecosystems, *Biogeosciences*, *6*, 405-429.
- Parsekian, A. D., L. Slater, D. Giménez (2012), Application of ground-penetrating radar to measure near-saturation soil water content in peat soils, *Water Resour. Res.*, *48*, W02533.
- Price, J. S., J. Cagampan, E. Kellner (2005), Assessment of peat compressibility: is there an easy way?, *Hydrol. Process.*, *19*(17), 3469-3475.
- Reid, M. C., R. Tripathy, K. V. R. Schäfer, P. R. Jaffé (2013), Tidal marsh methane dynamics: Difference in seasonal lags in emissions driven by storage in vegetated versus unvegetated sediments, *J. Geophys. Res. Biogeosci.*, doi:10.1002/jgrg.20152.
- Riutta, T., J. Laine, M. Aurela et al. (2007), Spatial variation in plant community functions regulates carbon gas dynamics in a boreal fen ecosystem, *Tellus B*, *59*(5), 838-852.
- Rosenberry, D. O., P. H. Glaser, D. I. Siegel, E. P. Weeks (2003), Use of hydraulic head to estimate volumetric gas content and ebullition flux in northern peatlands, *Water Resour. Res.*, *39*(3).
- Rothfuss, F. and R. Conrad (1998), Effect of gas bubbles on the diffusive flux of methane in anoxic paddy soil, *Limnol. & oceanogr.*, *43*(7), 1511-1518.

- Slater, L. D., and A. Reeve (2002), Investigating peatland stratigraphy and hydrogeology using integrated electrical geophysics, *Geophysics*, 67(2), 365-378.
- Slater, L., X. Comas, D. Ntarlagiannis, M. R. Moulik (2007), Resistivity-based monitoring of biogenic gases in peat soils, *Water Resour. Res.*, 43, W10430.
- Stamp, I., A. J. Baird, C. M. Heppell (2013), The importance of ebullition as a mechanism of methane (CH<sub>4</sub>) loss to the atmosphere in a northern peatland, *Geophys. Res. Lett.*, 40, 1-4.
- Stephen, K. D., J. R. M. Arah, K. L. Thomas, J. Benstead, D. Lloyd (1998a), Gas diffusion coefficient profile in peat determined by modelling mass spectrometric data: implications for gas phase distribution, *Soil Biol. & Biochem.*, 30(3), 429-431.
- Stephen, K. D., J. R. M. Arah, W. Daulat, R. S. Clymo (1998b), Root-mediated gas transport in peat determined by argon diffusion. *Soil Biol. & Biochem.*, 30(4), 501-508.
- Strack, M., E. Kellner, J. M. Waddington (2005), Dynamics of biogenic gas bubbles in peat and their effects on peatland biogeochemistry, *Glob. Biogeochem. Cycles*, 19, GB1003.
- Strack, M., and J. M. Waddington (2008), Spatiotemporal variability in peatland subsurface methane dynamics, *J. Geophys. Res.*, 113, G02010.
- Tang, J., Q. Zhuang, R. D. Shannon, J. R. White (2010), Quantifying wetland methane emissions with process-based models of different complexities. *Biogeosciences*, 7(4), 6121-6171.
- Tokida, T., T. Miyazaki, M. Mizoguchi (2005), Ebullition of methane from peat with falling atmospheric pressure, *Geophys. Res. Lett.*, 32, L13823.
- Tokida, T., T. Miyazaki, M. Mizoguchi, O. Nagata, F. Takakai, A. Kagemoto (2007), Falling atmospheric pressure as a trigger for methane ebullition from peatland, *Glob. Biogeochem. Cycles*, 21, GB2003.
- Tokida, T., T. Miyazaki, M. Mizoguchi (2009), Physical controls on ebullition losses of methane from peatlands. In: Baird, A., L. Belyea, X. Comas, A. Reeve, L. Slater (eds) *Northern peatlands and carbon cycling*, AGU, Washington, 219-228.
- Turetsky, M. R., C. C. Treat, M. P. Waldrop, J. M. Waddington, J. W. Harden, A. D. McGuire (2008), Short-term response of methane fluxes and methanogen activity to water table and soil warming manipulations in an Alaskan peatland, *J. Geophys. Res.*, 113, G00A10.

- Waddington, J. M., K. Harrison, E. Kellner, A. J. Baird (2009), Effect of atmospheric pressure and temperature on entrapped gas content in peat, *Hydrol. Process.*, 23, 2970-2980.
- Webb, E. K., G. I. Pearman, R. Leuning (1980), Correction of flux measurements for density effects due to heat and water vapour transfer, *Quart. J. R. Met. Soc.*, 106, 85-100.
- Wiesenburg, D. A. and N. L. Guinasso Jr. (1979), Equilibrium solubilities of methane, carbon monoxide, and hydrogen in water and sea water, *J. Chem. Eng. Data*, 24(4), 356-360.
- Williams, R. T. and R. L. Crawford (1984), Methane production in Minnesota peatlands, *Appl. Environ. Microbiol.*, 46(6), 1266-1271.
- Wuebbles, D. J., and K. Hayhoe, (2002), Atmospheric methane and global change, *Earth-Sci. Rev.*, 57(3), 177-210.
- Yoshikawa, K., W. R. Bolton, V. E. Romanovshy, M. Fukuda, L. D. Hinzman (2003), Impacts of wildfire on the permafrost in the boreal forests of Interior Alaska, *J. Geophys. Res.*, 108(D1), 8148.
- Zhang, Y., T. Sachs, C. Li, J. Boike (2012), Upscaling methane fluxes from closed chambers to eddy covariance based on a permafrost biogeochemistry integrated model, *Glob. Chang. Biol.*, 18, 1428-1440.

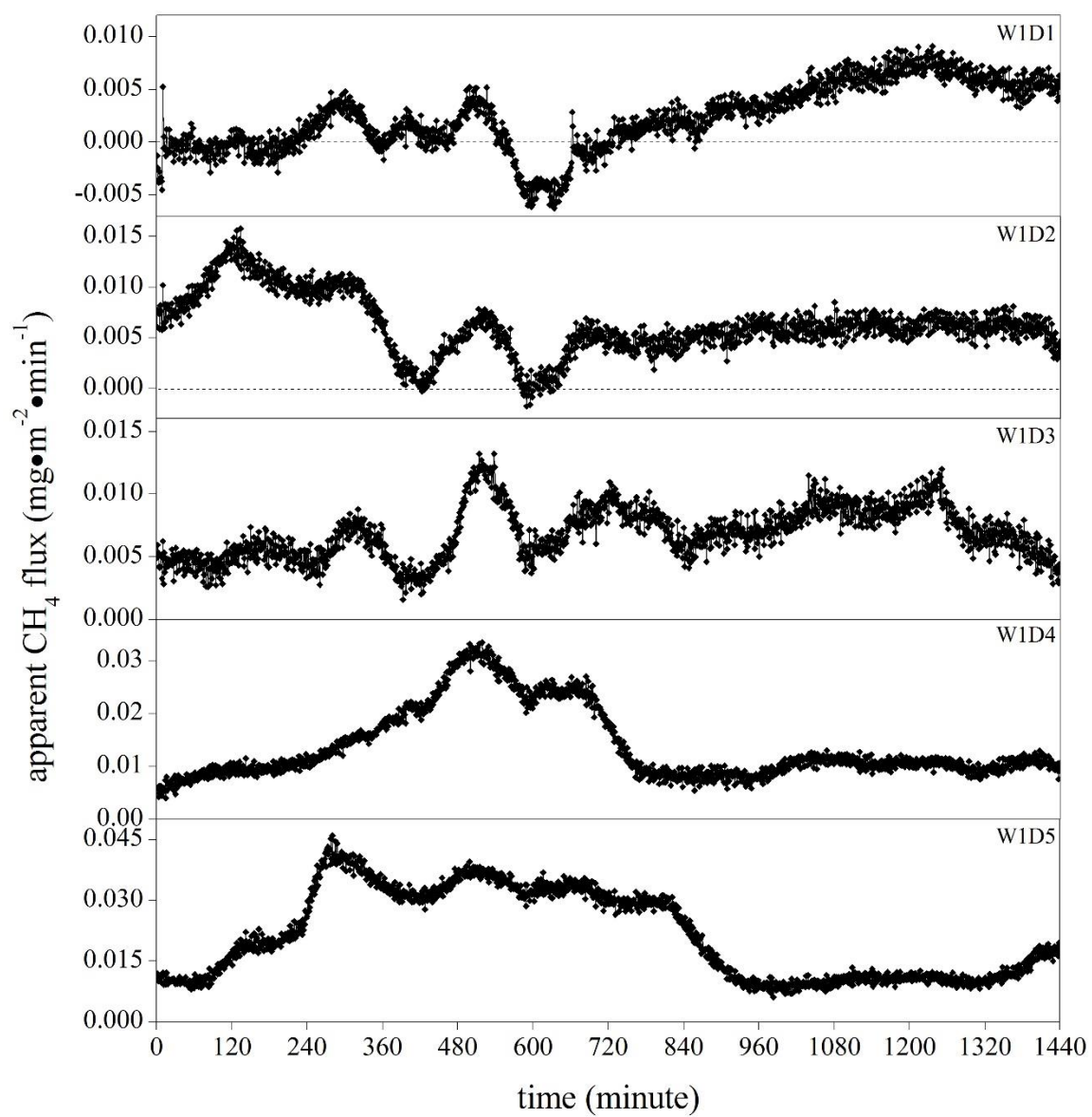
**Appendix: CH<sub>4</sub> flux data from DFC and CSC measurements**

Figure A1 CH<sub>4</sub> fluxes measured from DFC for the week 1. Note changes in scale of y axis.

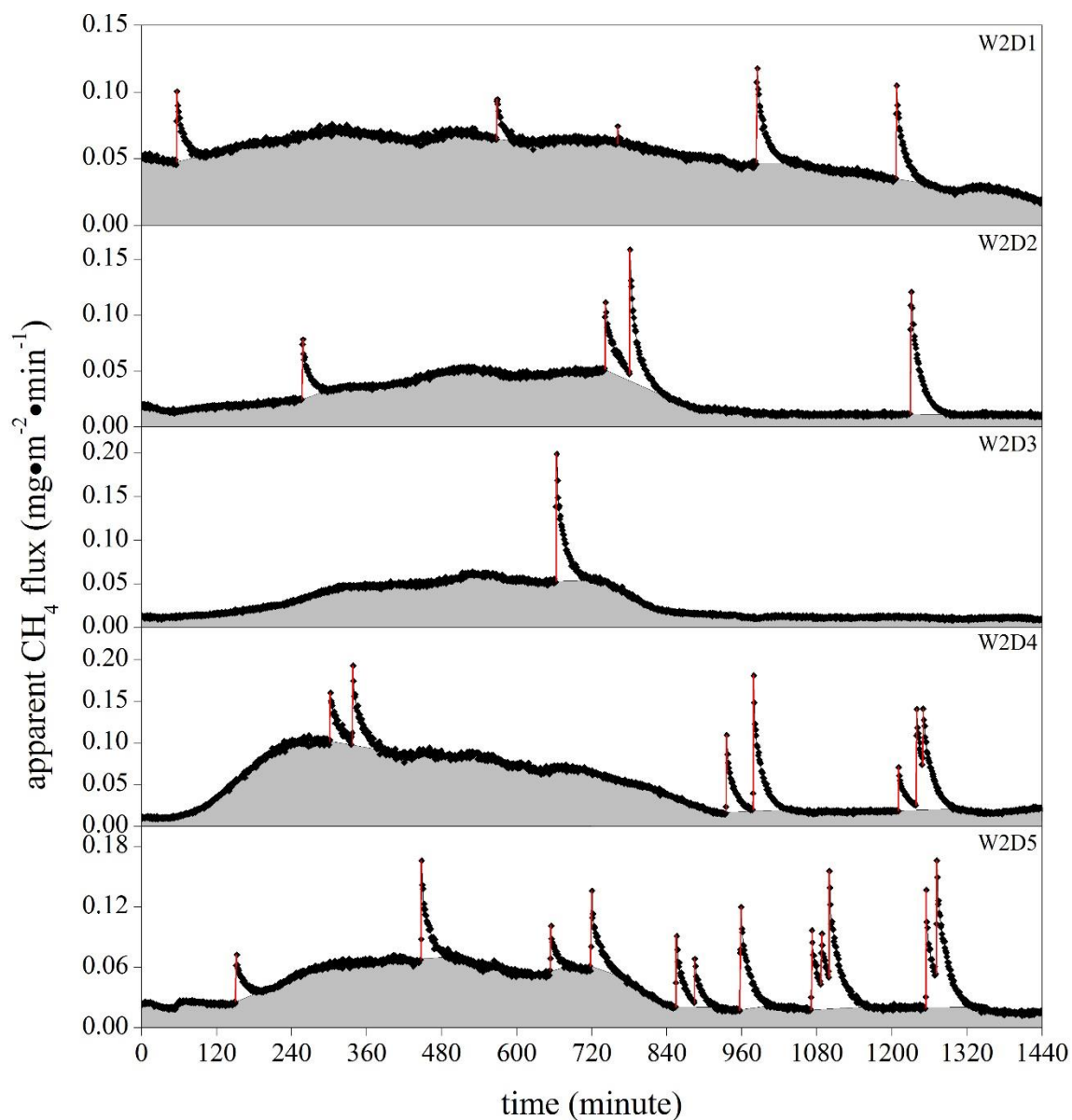


Figure A2 CH<sub>4</sub> fluxes measured from DFC for the week 2. Steady flux is shaded in gray, and ebullitive CH<sub>4</sub> releases are labeled in red lines. Note changes in scale of y axis.

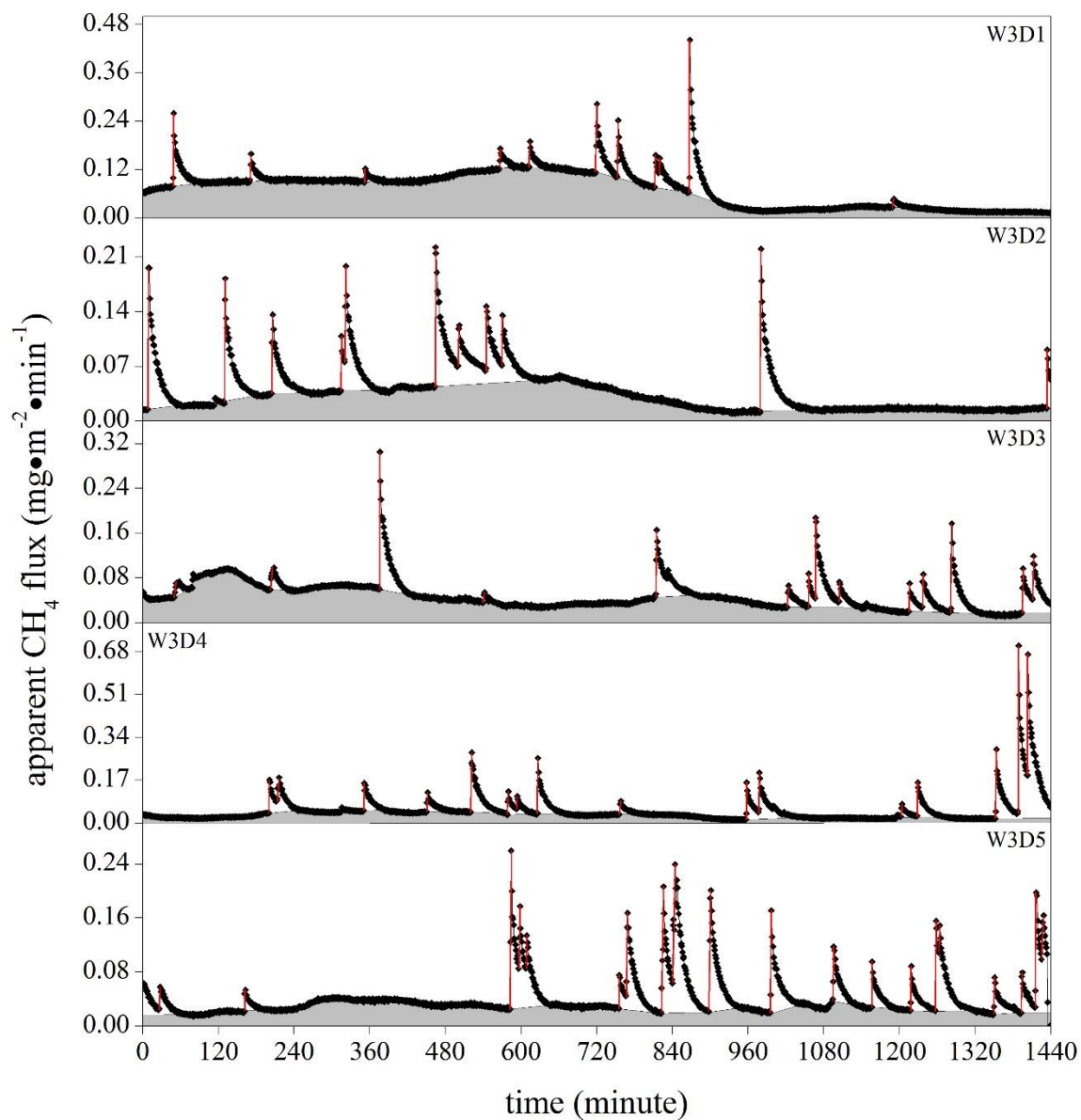


Figure A3 CH<sub>4</sub> fluxes measured from DFC for the week 3. Steady flux is shaded in gray, and ebullitive CH<sub>4</sub> releases are labeled in red lines. Note changes in scale of y axis.

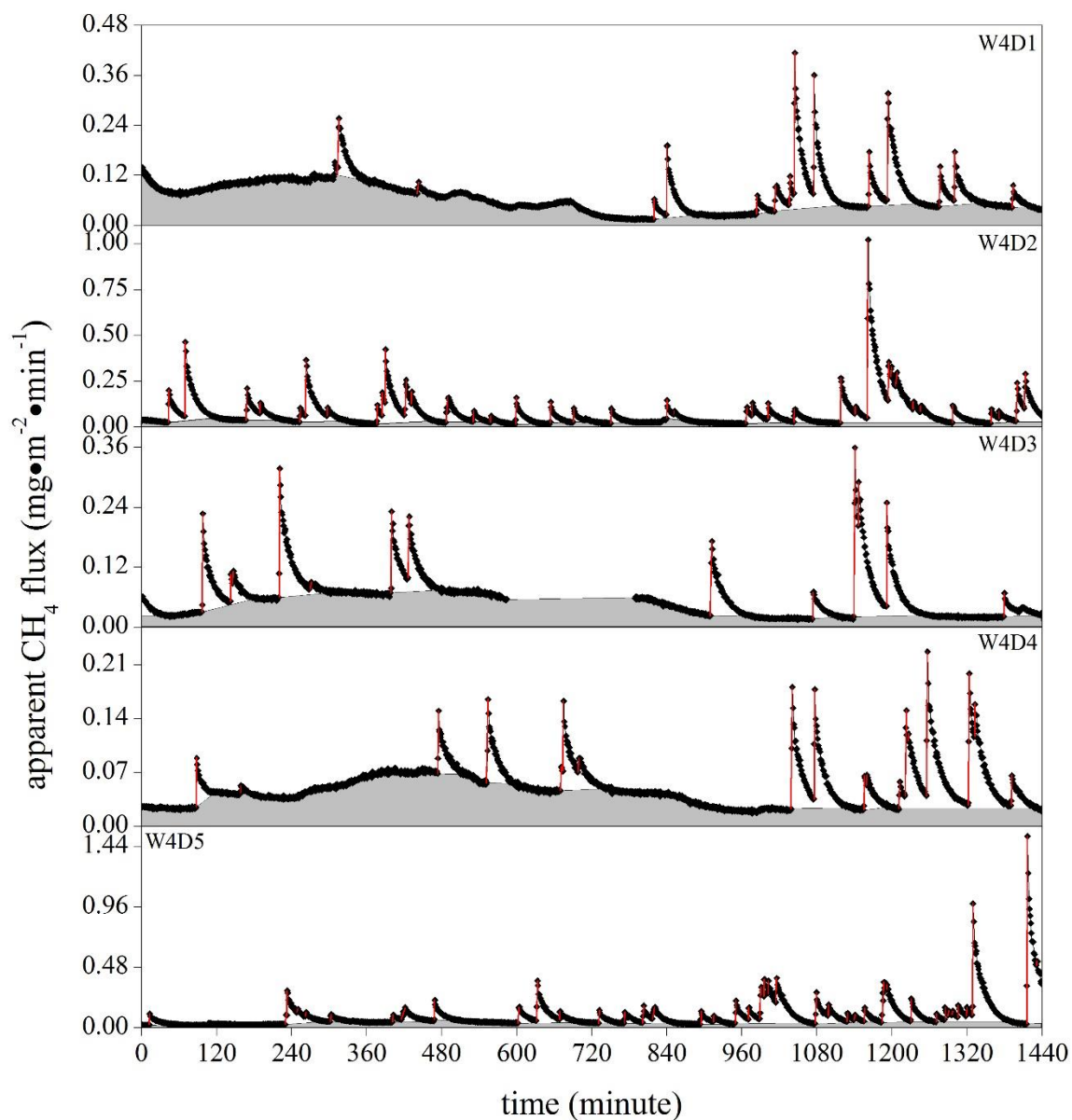


Figure A4  $\text{CH}_4$  fluxes measured from DFC for the week 4. Steady flux is shaded in gray, and ebullitive  $\text{CH}_4$  releases are labeled in red lines. The data gap in the fourth day was due to an electrical outage in the laboratory. Note changes in scale of y axis.

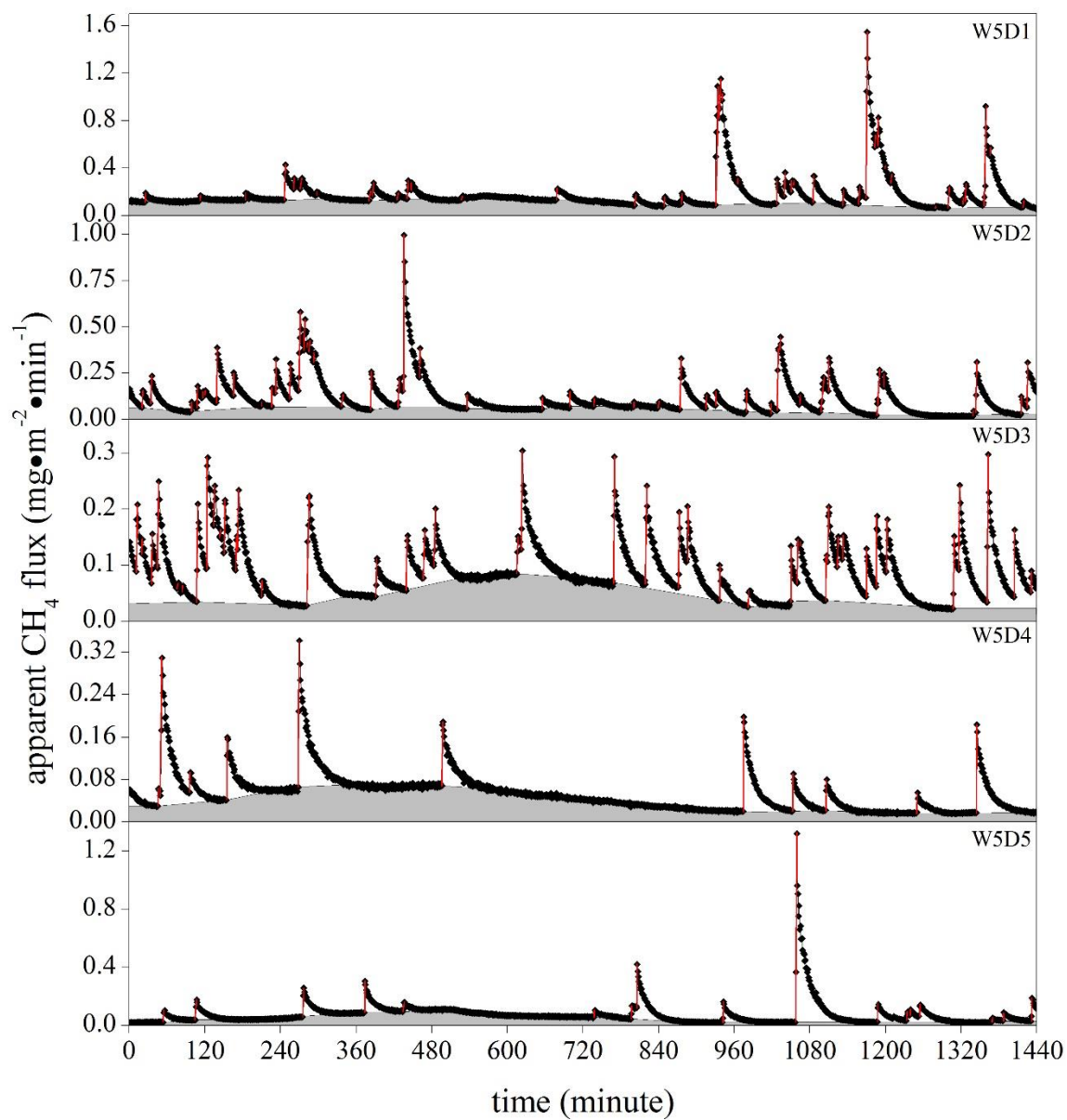


Figure A5 CH<sub>4</sub> fluxes measured from DFC for the week 5. Steady flux is shaded in gray, and ebullitive CH<sub>4</sub> releases are labeled in red lines. Note changes in scale of y axis.

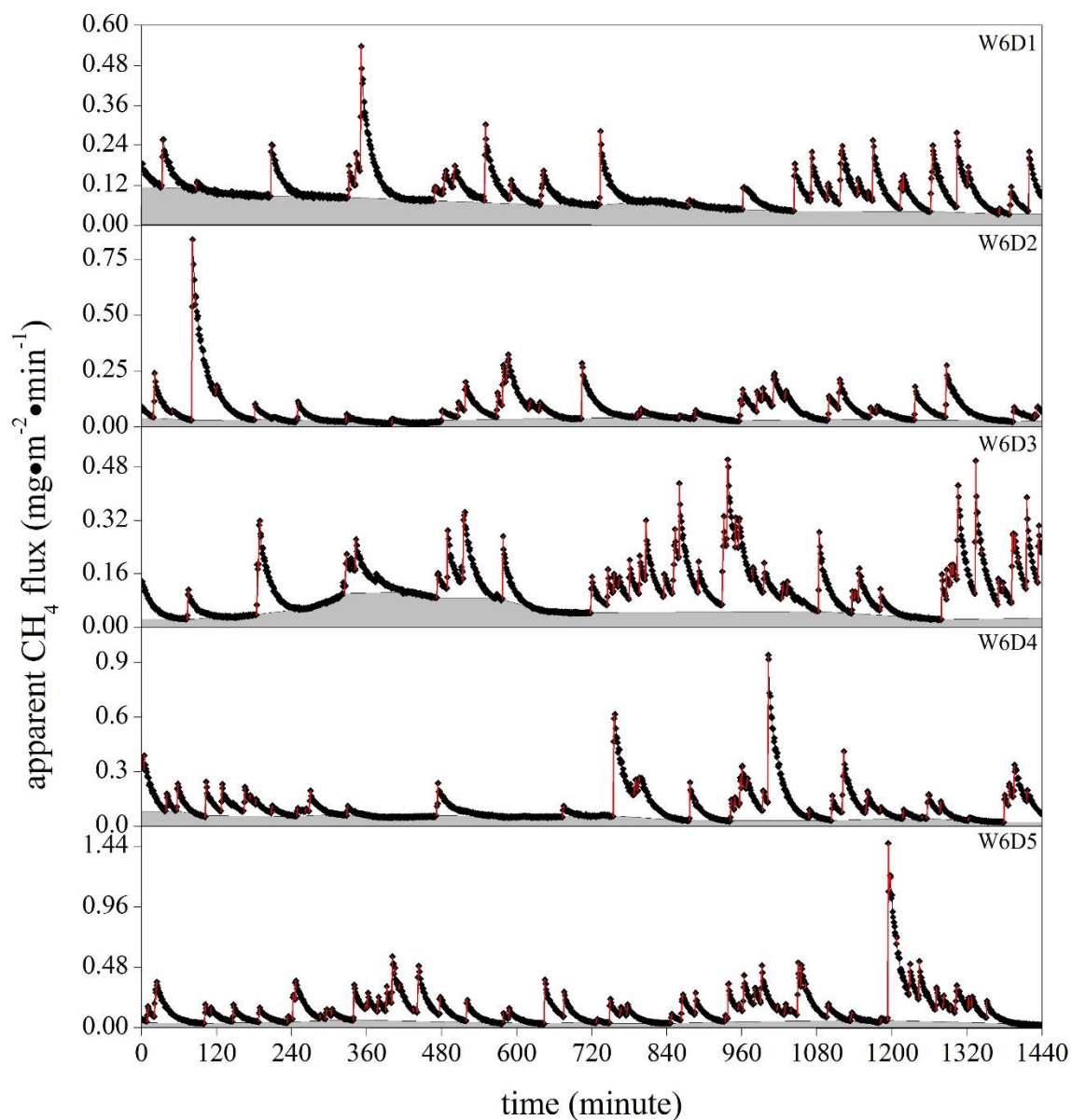


Figure A6 CH<sub>4</sub> fluxes measured from DFC for the week 6. Steady flux is shaded in gray, and ebullitive CH<sub>4</sub> releases are labeled in red lines. Note changes in scale of y axis.

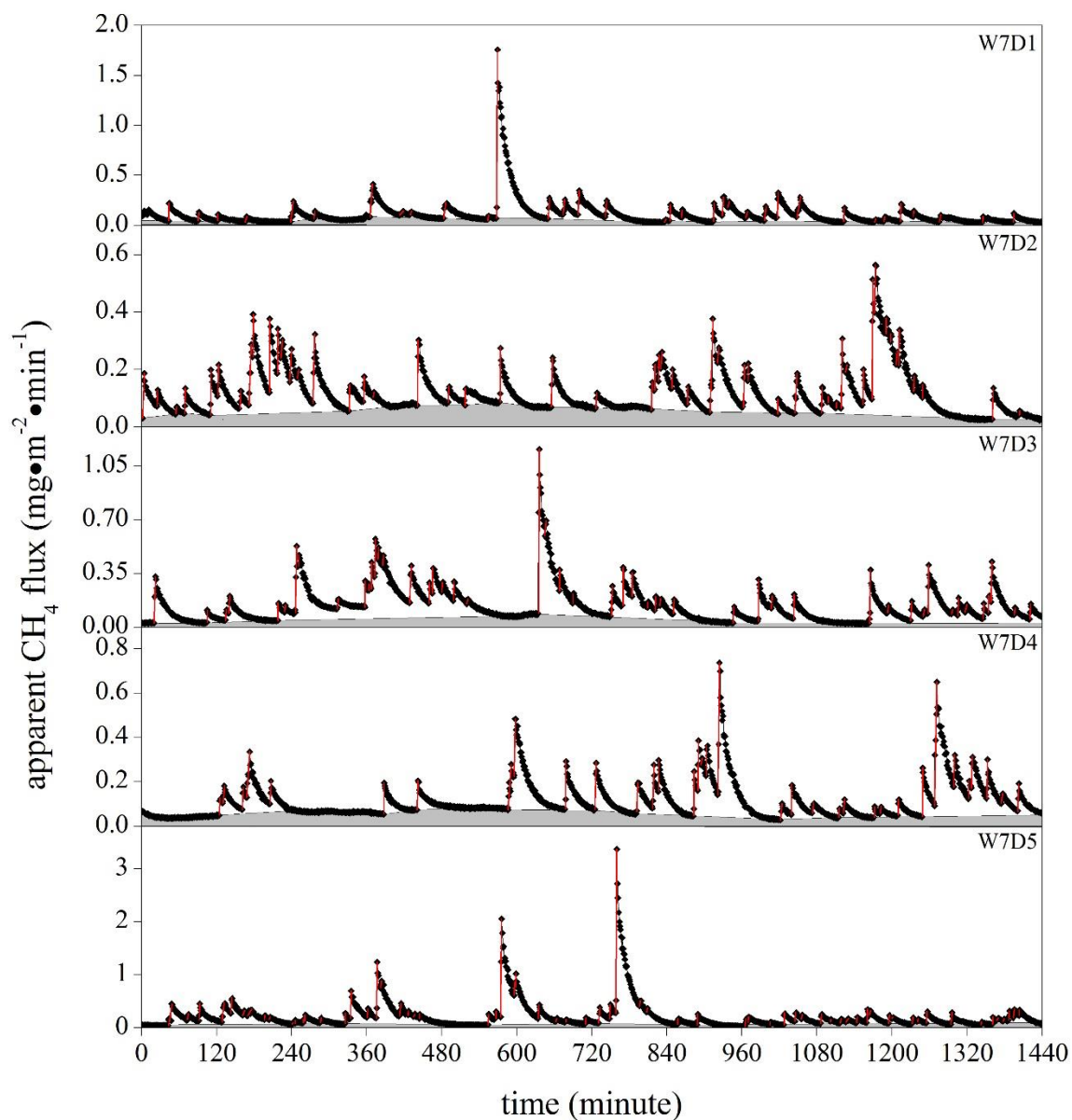


Figure A7 CH<sub>4</sub> fluxes measured from DFC for the week 7. Steady flux is shaded in gray, and ebullitive CH<sub>4</sub> releases are labeled in red lines. Note changes in scale of y axis.

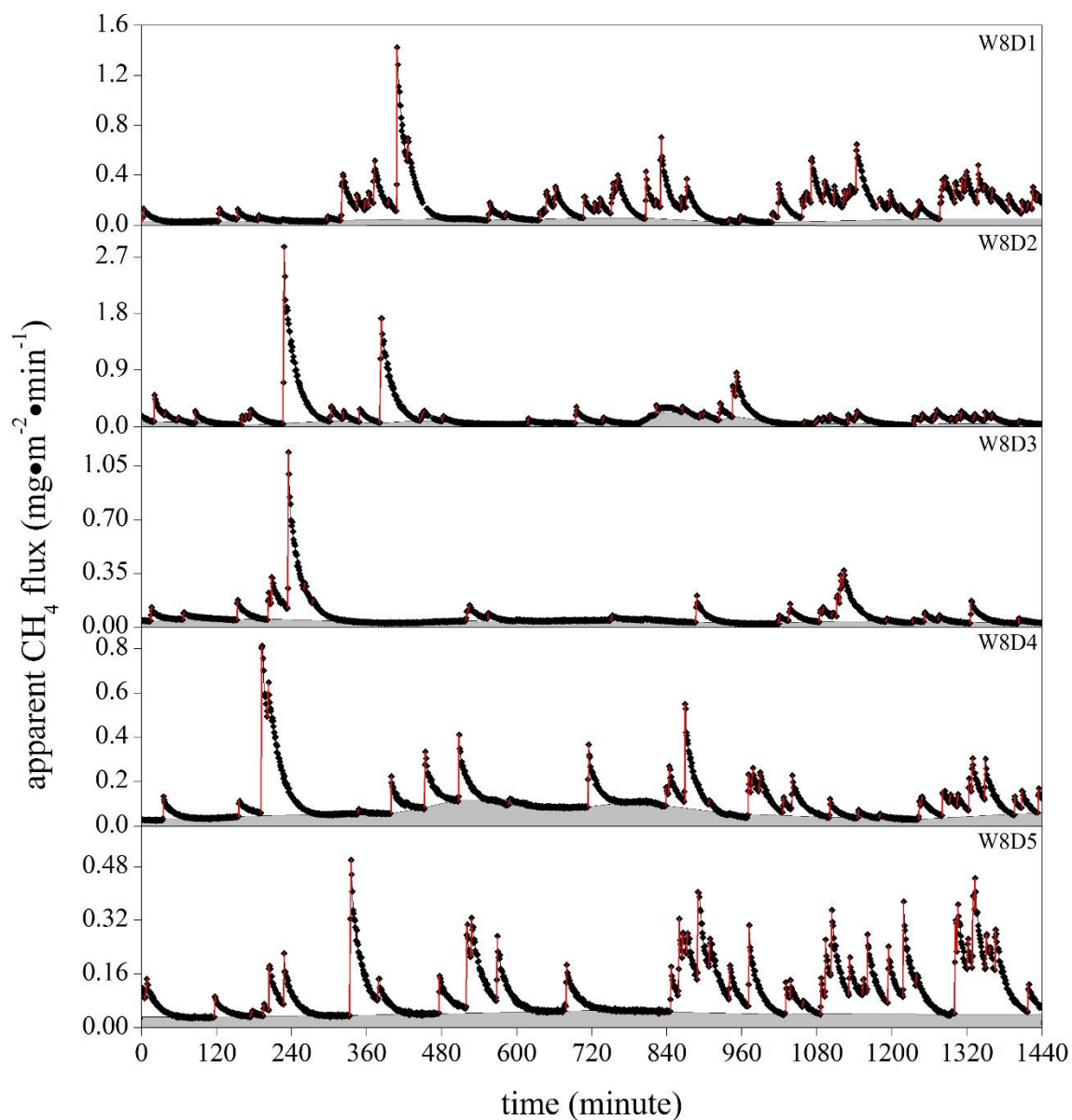


Figure A8 CH<sub>4</sub> fluxes measured from DFC for the week 8. Steady flux is shaded in gray, and ebullitive CH<sub>4</sub> releases are labeled in red lines. Note changes in scale of y axis.

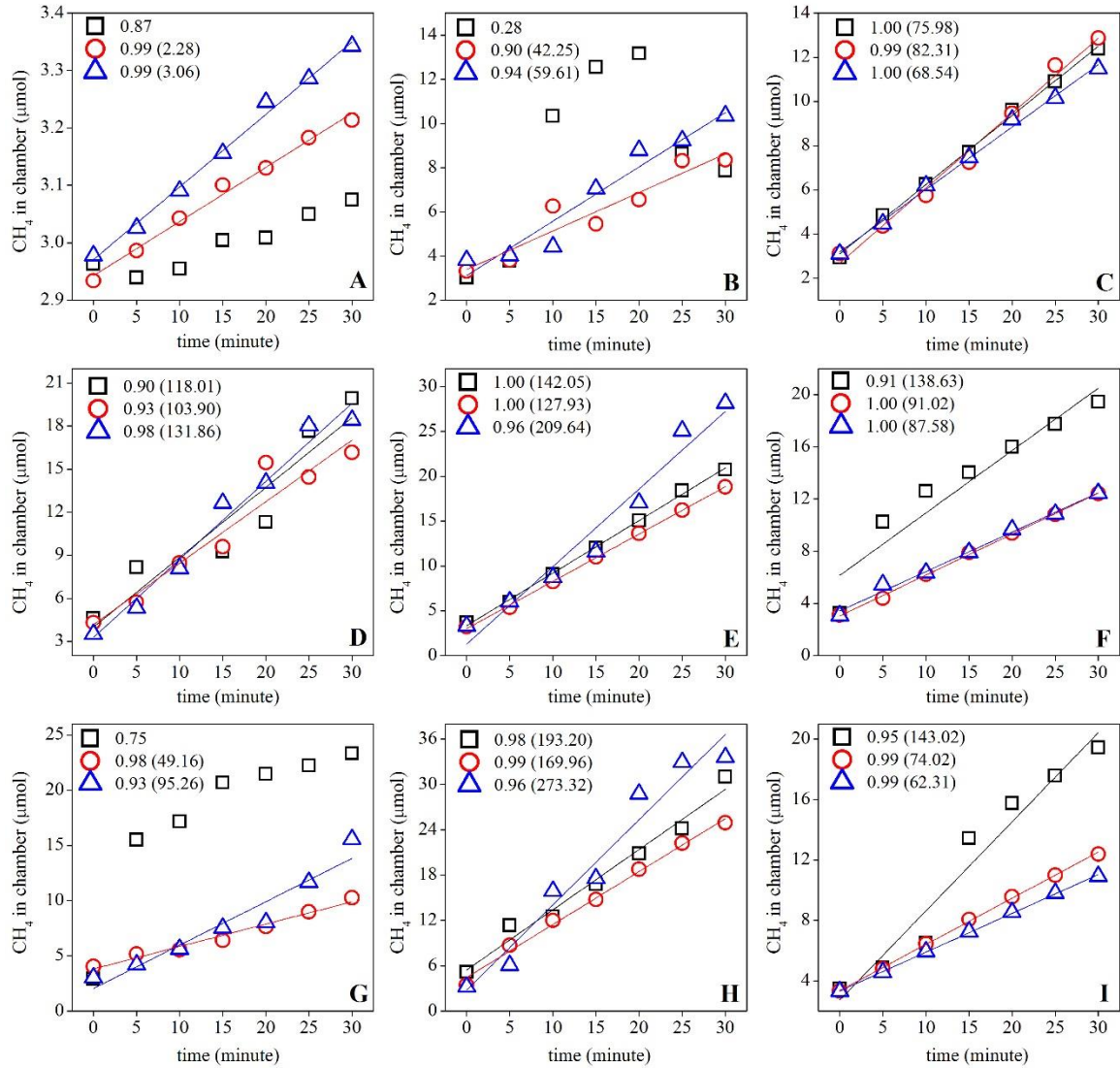


Figure A9 Calculation of CSC CH<sub>4</sub> flux using linear regression. (A) is for pre-incubation condition, and (B) to (I) are for CSC measurements taken after DFC measurement in every experimental week, respectively. Different symbols in each panel are replicate measurements. Coefficient of determination ( $R^2$ ) is shown in the legend. A criteria is set to be  $R^2 > 0.9$  for flux calculation. CSC CH<sub>4</sub> flux ( $\text{mg m}^{-2} \text{d}^{-1}$ ) from qualified dataset is shown in the bracket. Please note the changes in scale of the y-axis among different panels.

## **Curriculum vitae**

Date and place of birth: Feb. 7, 1986, Shanghai, China

M.S. Physical Geography (focus in Environmental Geochemistry), East China Normal University, Shanghai, China, 2011, advised by Dr. Dongqi Wang.

B.S. Geographical Sciences, East China Normal University, Shanghai, China, 2008, with Distinction.

Graduate Teaching Assistant, Dept. Earth and Environmental Sciences, Rutgers University, Newark, NJ (09/2011 – present).

Graduate Research Assistant, Dept. Geography, East China Normal University, Shanghai, China (09/2008 - 06/2011).

Excellent Master Dissertation. East China Normal University, Shanghai, China, (2011) Dissertation Fellowship. Graduate School, East China Normal University, Shanghai, China, (2010-2011).

First Grade Academic Scholarship. Dept. Geography, East China Normal University, Shanghai, China, (2008-2011).

Excellent Graduates. Shanghai Ministry of Education, (2008).

Excellent Bachelor Dissertation. East China Normal University, China, (2008)

Full Tuition Scholarship. Dept. Geography, East China Normal University, Shanghai, China, (2004-2008).

## Publication:

1. **Yu, Z.**, H. Deng, D. Wang, M. Ye, Y. Tan, Y. Li, Z. Chen, and S. Xu. 2013. Nitrous oxide emissions in the Shanghai river network: implications for the effects of urban sewage and IPCC methodology. Global Change Biology. doi: 10.1111/gcb.12290.
2. Zhou D., C. Bi, Z. Chen, **Z. Yu**, J. Wang, J. Han. 2013. Phosphorus loads from different urban storm runoff sources in southern China: a case study in Wenzhou City. Environmental Science and Pollution Research, 1-10.
3. **Yu, Z.**, Y. Li, H. Deng, D. Wang, Z. Chen, and S. Xu. 2012. Effect of *Scirpus mariqueter* on nitrous oxide emissions from a subtropical monsoon estuarine wetland. Journal of Geophysical Research-Biogeosciences, 117, G02017.
4. **Yu, Z.**, D. Wang, Z. Chen, Y. Qi, Z. Nie, S. Xu. 2011. Purification of eutrophic river water in artificial floating beds combined with carriers. China Water & Wastewater, 27(17), 31-35. (in Chinese with English abstract)
5. Sun, C., C. Bi, Z. Chen, D. Wang, C. Zhang, Y. Sun, **Z. Yu**, D. Zhou. 2010. Assessment on environmental quality of heavy metals in agricultural soils of Chongming Island, Shanghai City. Journal of Geographical Sciences, 20, 135-147.